

OPTIMIZATION OF TRANSPORT PROPERTIES OF
POLY (ACRYLAMIDE-CO-ACRYLIC ACID) BASED
POLYMER ELECTROLYTES

SAMINATHA KUMARAN A/L VELOO

FACULTY OF SCIENCE
UNIVERSITI MALAYA
KUALA LUMPUR

2022

**OPTIMIZATION OF TRANSPORT PROPERTIES OF
POLY (ACRYLAMIDE-CO-ACRYLIC ACID) BASED
POLYMER ELECTROLYTES**

SAMINATHA KUMARAN A/L VELOO

**DISSERTATION SUBMITTED IN FULFILMENT OF
THE REQUIREMENTS FOR THE DEGREE OF
MASTERS OF SCIENCE**

**DEPARTMENT OF PHYSICS
FACULTY OF SCIENCE
UNIVERSITI MALAYA
KUALA LUMPUR**

2022

UNIVERSITI MALAYA
ORIGINAL LITERARY WORK DECLARATION

Name of Candidate: **Saminatha kumaran A/L Veloo**

Matric No: **17007476**

Name of Degree: **Masters of Science**

Title of Dissertation (“this Work”):

Optimization of Transport Properties of Poly (Acrylamide-Co-Acrylic Acid) Based Polymer Electrolytes

Field of Study: **Experimental Physics**

I do solemnly and sincerely declare that:

- (1) I am the sole author/writer of this Work;
- (2) This Work is original;
- (3) Any use of any work in which copyright exists was done by way of fair dealing and for permitted purposes and any excerpt or extract from, or reference to or reproduction of any copyright work has been disclosed expressly and sufficiently and the title of the Work and its authorship have been acknowledged in this Work;
- (4) I do not have any actual knowledge nor do I ought reasonably to know that the making of this work constitutes an infringement of any copyright work;
- (5) I hereby assign all and every rights in the copyright to this Work to the University of Malaya (“UM”), who henceforth shall be owner of the copyright in this Work and that any reproduction or use in any form or by any means whatsoever is prohibited without the written consent of UM having been first had and obtained;
- (6) I am fully aware that if in the course of making this Work I have infringed any copyright whether intentionally or otherwise, I may be subject to legal action or any other action as may be determined by UM.

Candidate’s Signature

Date: 14.02.2022

Subscribed and solemnly declared before,

Witness’s Signature

Date: 14.02.2022

Name:

Designation:

**OPTIMIZATION OF TRANSPORT PROPERTIES OF POLY
(ACRYLAMIDE-CO-ACRYLIC ACID) BASED POLYMER ELECTROLYTES**

ABSTRACT

Over the last few decades, transport properties of solid polymer electrolytes play vital role in variety of electrochemical devices such as high energy density batteries, super capacitors, fuel cells, sensors, and dye-sensitized solar cells. Generally, solid polymer electrolytes have several advantages such as leakage-proof, lightweight, improved safety, inexpensive, good thermal stability, high flexibility, and ease of fabrication. In this research work, polymer electrolyte thin films based on Poly (acrylamide-co-acrylic acid) (PAAC) doped with Sodium Iodide (NaI) (System A) and system B was prepared by adding ionic liquid of 1-Butyl-3-Methylimidazolium Iodide (BMI) with optimized PAAC-NaI system in different ratios of polymer, salt, and ionic liquid by using solution casting method. In both Systems A and B, a fixed amount of additive of Propylene Carbonate (PC) was added to polymer electrolyte systems. The Propylene Carbonate (PC) was added to the mixture of the solution to provide more flexibility to the polymer film by increasing the plasticity of the thin film membrane. The conductivity and dielectric studies were carried out on these thin films over the wide range of frequencies from 50 Hz to 5 MHz to understand the ionic transport properties of the polymer electrolytes. The highest ionic conductivity has been found to be $1.88 \times 10^{-5} \text{ Scm}^{-1}$ for the system A optimized with 30 wt.% of NaI salt-doped polymer electrolyte system at room temperature and maximum ionic conductivity of $4.73 \times 10^{-4} \text{ S cm}^{-1}$ achieved for system B containing the optimized 30 wt. % NaI salt-doped polymer electrolyte and 15 wt.% BMI ionic liquid at room temperature. For both systems, the temperature dependent ionic conductivity agreed with Arrhenius relationship which shows the ion hopping mechanism of ions in the polymer matrix. The dielectric properties especially the loss tangent was analyzed to observe the segmental relaxation of the polymer chain upon incorporation of

salt and ionic liquid. Further investigations were made to analyze the behaviour of thermally activated ionic diffusion and its overall effect on segmental dynamics of solid polymer electrolyte systems.

Keywords: Impedance Spectroscopy, Dielectric, Modulus Electric, Loss Tangent and Segmental Relaxation

Universiti Malaya

PENGOPTIMUMAN CIRI-CIRI PENGANGKUTAN DALAM POLY (ACRYLAMIDE-CO-ACRYLIC ACID) BERASASKAN ELEKTROLIT POLIMER

ABSTRAK

Sejak beberapa dekad yang lalu, ciri-ciri pengangkutan dalam elektrolit polimer pepejal memainkan peranan yang amat penting dalam pelbagai aplikasi peranti elektrokimia seperti sel kering berketumpatan tinggi, kapasitor berkeupayaan tinggi, sel bahan api, alat pengesan, and sel solar peka pewarna. Secara umumnya elektrolit polimer pepejal mempunyai beberapa kelebihan seperti kalis kebocoran, ringan, ciri-ciri keselamatan yang diperbaiki, murah, kestabilan terma yang lebih baik, kebolehlenturan yang tinggi dan mudah untuk fabrikasi. Dalam penyelidikan ini sistem A, elektrolit polimer pepejal berbentuk filem nipis disediakan dengan polimer hos, Polyacrylamide-co-acrylic acid (PAAC) didopkan dengan garam Sodium Iodide (NaI) dan turut disediakan sistem B, dimana larutan ionic 1-Butyl-3-Methylimidazolium Iodide (BMI) ditambahkan ke dalam system PAAC-NAI yang dioptimumkan mengikut nisbah urutan yang teratur dengan kaedah penyediaan larutan "casting". Dalam kedua-dua sistem A dan B, aditif Propylene Carbonate (PC) ditambah dengan nisbah yang tetap. Di mana Propylene Carbonate (PC) ditambah kedalam larutan sebatil tersebut supaya agar memberikan kelenturan yang optimum kepada filem polimer dengan menambahkan sifat keplastikan kepada membran filem tersebut. Kajian kekonduksian dan dielektrik dikendalikan keatas filem nipis dalam julat frekuensi yang lebar dari 50 Hz hingga 5 MHz, untuk memahami ciri-ciri pengangkutan dalam elektrolit polimer secara teliti. Kekonduksian yang optimum dicapai adalah $1.88 \times 10^{-5} \text{ Scm}^{-1}$ bagi system A pada suhu bilik bagi nisbah 30% garam NaI didopkan ke dalam system PAAC-NaI elektrolit polimer dan kekonduksian terbaik dicapai adalah $4.73 \times 10^{-4} \text{ S cm}^{-1}$ bagi sistem B pada suhu bilik bagi nisbah 15% larutan ionic BM ditambah dengan sistem PAAC-NaI elektrolit polimer. Dimana sifat kekonduksian yang bersandar kepada terma suhu mematuhi hubungkait Arrhenius yang menunjukkan

mekanisme lompatan ion di dalam kekisi matriks polimer yang menandakan kekonduksian elektrik. Cir-ciri dielektrik terutamanya “loss tangent” digunakan untuk mengkaji sifat relaksasi segmen rantai polimer dengan penambahan garam dengan nisbah urutan yang meningkat. Penyelidikan yang selanjutnya dilakukan untuk menganalisa sifat difusi ion yang bersandar kepada perubahan suhu terma dan kesan secara keseluruhannya kepada dinamik segmen dalam sistem elektrolit polimer pepejal.

Kata Kunci: Spektroskopi Impedans, Dielektrik, Modulus Elektrik, Sifat Relaksasi Segmental

Universiti Malaysia

ACKNOWLEDGEMENTS

First and foremost, I am extremely grateful to my supervisors, Prof. Dr. Ramesh Subramaniam and Dr. Vengadaesvaran Balakrishnan for the continuous support and invaluable supervision, and tutelage during the course of my MSc postgraduate program to enhance the quality of my research work, and immense knowledge. Additionally, I would like to express sincere gratitude to Associate Prof. Dr. Ramesh Kasi for always providing treasured knowledge and keeps motivating throughout my postgraduate studies. I likewise express my earnest gratitude to Dr. Numan Arshid, Dr. Shahid Bashir and Dr. Hon Ming for their intellectual help during my research and provided me support in shaping my experiment methods and guided throughout my preparation of manuscript for my journal publication and thesis. I would like to extend my gratitude to Dr. Fatin Saiha, Dr. Amar, Mr. Surender Gunalan, Dr. Mohd Zahurin for their valuable scientific discussions, and always willingly to helping me out their technical support on my study.

Also I would like to thank my lab fellows/seniors members/research students of Center for Ionics and Department of Physics for providing me space to work in the lab with good positive vibration throughout my experimental studies. Finally, a deepest gratitude goes to my loving family, my wife, and my children. Without their tremendous understanding, encouragement and sacrifices in the past few years, it would be impossible for me to complete my postgraduate studies. Your prayer for me was what sustained me this far. **I would like to dedicate this work to my Father Mr. Veloo Alagunadar & my Mother Madam Mookammal Solaimalai**, whose prayers always protect and provide a driving force in me in every difficult situation.

SAMINATHA KUMARAN VELOO

TABLE OF CONTENTS

| | |
|--|-------------|
| ABSTRACT | iii |
| ABSTRAK | v |
| ACKNOWLEDGEMENTS | vii |
| TABLE OF CONTENTS | viii |
| LIST OF FIGURES | xi |
| LIST OF TABLES | xiii |
| LIST OF SYMBOLS AND ABBREVIATIONS | xiv |
| | |
| CHAPTER 1: INTRODUCTION | 1 |
| 1.1 Background of the research | 1 |
| 1.2 Problems Statements..... | 3 |
| 1.3 Aims and Objectives of Research..... | 3 |
| 1.4 Outline of Thesis..... | 4 |
| | |
| CHAPTER 2: LITERATURE REVIEW | 6 |
| 2.1 Solid Polymer Electrolytes | 6 |
| 2.2 General Description of Ionic Conduction Mechanism | 7 |
| 2.2.1 Electrochemical Impedance Spectroscopy | 8 |
| 2.2.2 DC Conductivity and Temperature Dependent Conductivity | 10 |
| 2.3 Methods to Enhance the Ionic Conduction Mechanism | 11 |
| 2.3.1 Effects of Adding Salt, Ionic Liquids and Plasticizers..... | 11 |
| 2.4 Dielectric Properties and Fundamental of Electric Modulus..... | 12 |
| 2.4.1 Dielectric constant and Dielectric Loss | 13 |
| 2.4.2 Loss Tangent Spectra and Relaxation Time..... | 15 |
| 2.4.3 Electric Modulus | 17 |

| | | |
|---|--|-----------|
| 2.5 | Transport Properties and Diffusion Model for Ionic Conductivity | 19 |
| 2.5.1 | Transport Model Analysis | 19 |
| 2.5.2 | Relationship between carrier charge density (n), ionic mobility (μ) and diffusion coefficient (D) | 20 |
| CHAPTER 3: METHODOLOGY | | 22 |
| 3.1 | Materials and Sample Preparation | 22 |
| 3.2 | Characterization | 25 |
| 3.2.1 | X-Ray Diffraction Analysis | 25 |
| 3.3 | Electrochemical Impedance Spectroscopy (EIS) Analysis | 25 |
| CHAPTER 4: RESULTS AND DISCUSSION | | 27 |
| 4.1 | Characterization | 27 |
| 4.1.1 | Structural Characterization (X-Ray Diffraction Analysis) | 27 |
| 4.2 | Ionic Conductivity and Activation Energy | 29 |
| 4.2.1 | Temperature Dependence Arrhenius behavior of Ionic Conductivity | 32 |
| 4.3 | The Broadband Dielectric Spectroscopy Analysis | 35 |
| 4.3.1 | Temperature Dependent Dielectric Spectra | 37 |
| 4.3.2 | Tangent Loss Spectra Analysis at room temperature | 39 |
| 4.3.3 | Temperature Dependent Tangent Loss Spectra Analysis | 42 |
| 4.3.4 | Modulus Electric Analysis at room temperature | 45 |
| 4.3.5 | Temperature Dependent Modulus Electric Analysis | 47 |
| CHAPTER 5: CONCLUSIONS AND FUTURE WORK | | 49 |
| 5.1 | Conclusions | 49 |
| 5.2 | Future Work | 49 |

| | |
|--|-----------|
| REFERENCES..... | 51 |
| LIST OF PUBLICATIONS AND PAPERS PRESENTED | 57 |

Universiti Malaya

LIST OF FIGURES

| | |
|---|----|
| Figure 2.1 : Impedance Plot of Z_{img} versus Z_{real} to exhibit bulk resistance R_b (Aziz et al., 2018)..... | 9 |
| Figure 2.2 : Dielectric Constant ϵ' and Dielectric Loss ϵ'' versus $\log f$ plot over broad range frequency (Sangeetha et al., 2021)..... | 14 |
| Figure 2.3 : Loss Tangent $\tan\delta$ versus $\log f$ plot over broad range frequency (Koops, 1951)..... | 16 |
| Figure 2.4 : Modulus electric real M' and Modulus electric imaginary M'' versus $\log f$ plot over broad range frequency (Woo et al., 2012)..... | 18 |
| Figure 3.1 : (a), (b) and (c) System A [PAAC-NaI] solutions stir uniformly with magnetic stirrer and the casted solution after stir 24 hours respectively. | 24 |
| Figure 3.2 : Free standing solid film after dried in oven at 60 °C for System B. | 24 |
| Figure 3.3 : The clear and transparent solid electrolyte film peel off from petri dish. ... | 25 |
| Figure 3.4 : (a) The two-electrode parallel blocking stainless steel electrodes plate configuration system & (b) The prepared samples sandwiched between the sample holders. | 26 |
| Figure 4.1 : X-Ray diffractogram of (a) sodium iodide and (b) solid polymer electrolyte thin films. | 29 |
| Figure 4.2 : Log (conductivity) and activation energy plots of different [PAAC-NaI] electrolyte system. | 30 |
| Figure 4.3 : Log (conductivity) and activation energy plots of different [PAAC-NaI-BMI] electrolyte system. | 32 |
| Figure 4.4 : Temperature dependent ionic conductivity of different [PAAC-NaI] electrolyte system A. | 33 |
| Figure 4.5 : Temperature dependent ionic conductivity of different [PAAC-NaI-BMI] electrolyte system B..... | 34 |
| Figure 4.6 : The (a) ϵ' versus $\log f$ and (b) ϵ'' versus $\log f$, plots of different [PAAC-NaI] electrolyte system A at room temperature..... | 36 |
| Figure 4.7 : The (a) ϵ' versus $\log f$ and (b) ϵ'' versus $\log f$, plots of different [PAAC-NaI -BMI] electrolyte system B at room temperature. | 36 |

| | |
|--|----|
| Figure 4.8 : The temperature dependent (a) ϵ' versus $\log f$ and (b) ϵ'' versus $\log f$ respectively for optimized N30 electrolyte system A..... | 38 |
| Figure 4.9 : The temperature dependent (a) ϵ' versus $\log f$ and (b) ϵ'' versus $\log f$ respectively for optimized BMI15 electrolyte system B. | 38 |
| Figure 4.10 : Variation of loss tangent versus $\log f$ plot for (a) System A and (b) System B respectively at room temperature. | 40 |
| Figure 4.11 : Variation of loss tangent versus $\log f$ plot for (a) System A and (b) System B respectively at 313 K..... | 42 |
| Figure 4.12 : Variation of loss tangent versus $\log f$ plot for (a) System A and (b) System B respectively at 323 K..... | 43 |
| Figure 4.13 : Variation of loss tangent versus $\log f$ plot for (a) System A and (b) System B respectively at 333K..... | 43 |
| Figure 4.14 : Variation of loss tangent versus $\log f$ plot for (a) System A and (b) System B respectively at 343K..... | 44 |
| Figure 4.15 : Variation of loss tangent versus $\log f$ plot for (a) System A and (b) System B respectively at 353K..... | 44 |
| Figure 4.16 : Variation of loss tangent versus $\log f$ plot for (a) System A and (b) System B respectively at 363K..... | 44 |
| Figure 4.17 : Variation of loss tangent versus $\log f$ plot for (a) System A and (a) System B respectively at 373K..... | 45 |
| Figure 4.18 : Variation of (a) M' versus $\log f$ and (b) Variation of M'' versus $\log f$ for different [PAAC-NaI] electrolyte system A at room temperature..... | 46 |
| Figure 4.19 : Variation of (a) M' versus $\log f$ and (b) Variation of M'' versus $\log f$ for different [PAAC-NaI-BMI] electrolyte system B at room temperature. | 46 |
| Figure 4.20 : The temperature dependent (a) M' versus $\log f$ and (b) M'' versus $\log f$ respectively for optimized N30 electrolyte system A..... | 48 |
| Figure 4.21 : The temperature dependent (a) M' versus $\log f$ and (b) M'' versus $\log f$ respectively for optimized BMI15 electrolyte system B. | 48 |

LIST OF TABLES

| | |
|--|----|
| Table 3.1 : The Compositions of the System A: PAAC-NaI polymer electrolyte..... | 23 |
| Table 3.2 : The Compositions of the System B: PAAC - NaI - BMI polymer electrolyte..... | 23 |
| Table 4.1 : The peak frequency, f_m and the relaxation time, τ for system A..... | 41 |
| Table 4.2 : The peak frequency, f_m and the relaxation time, τ for system B..... | 42 |

Universiti Malaya

LIST OF SYMBOLS AND ABBREVIATIONS

| | | |
|------|---|--|
| AC | : | Alternating Current |
| BMI | : | 1-Butly-3-Methylimidazolium Iodide |
| DC | : | Direct Current |
| EIS | : | Electrochemical Impedance Spectroscopy |
| NaI | : | Sodium Iodide |
| NMR | : | Nuclear Magnetic Resonance |
| PAC | | Polyacrylic acid |
| PAM | | Polyacrylamide |
| PAAC | : | Poly (acrylamide-co-acrylic acid) |
| PC | : | Propylene Carbonate |
| SPE | : | Solid Polymer Electrolytes |
| UM | : | Universiti Malaya |
| XRD | | X-Ray Diffractometer |

CHAPTER 1: INTRODUCTION

Solid polymer electrolyte thin films are solid ionic conductors that are formed by the dissolution of salts in suitable high molecular weight polymers and naturally possess better chemical stability and mechanical strength. Due to rigorous study driven by their prospective uses in various electrochemical device applications, the solid polymer electrolyte conductors undergone revolutionary research and development in the past few decades. However, enhanced solid polymer electrolyte transport characteristics are required to optimize the performance of the electrochemical device applications.

1.1 Background of the research

The most promising technique for understanding the ion dynamics and relaxation behavior of solid polymer electrolyte systems is the experimental analysis of transport properties. There are three important basic transport properties that were analyzed in this work; ionic conductivity, dielectric spectroscopy, and diffusion parameters. These basic properties play an important role especially in the optimization of the solid polymer electrolytes in a variety of electrochemical devices such as high energy density batteries, supercapacitors, fuel cells, electrochemical sensors, and dye-sensitized solar cells (Agrawal & Pandey, 2008; Singh et al., 2010; Wang, 2009) and quantum dots-based application devices (Singh et al., 2009).

Generally, solid polymer electrolytes have advantages in commercialization due to their longer lifetime and high thermal stability, mechanical strength, naturally abundant sources of synthesis and cost effectiveness. Therefore, it can be easily fabricated as thin film and has ability to form good electrode/electrolyte contacts. Compared to other types of aqueous electrolytes, solid polymer electrolytes have very limited problem in leakage or pressure distortion (Avellaneda et al., 2007).

In this work, a solid polymer electrolyte based on Poly (acrylamide-co-acrylic acid) (PAAC) copolymer was synthesized where PAAC was used as the host polymer. In general, copolymers combines the chemical and physical properties of its constituent polymers. Polyacrylamide (PAM) is a water-soluble polymer that has been extensively researched due to its advantages as a binder and filler for improving conductivity, as well as its excellent electrical-thermal properties, which make it suitable for a wide range of electrochemical device applications (Wieczorek et al., 1995). Polyacrylic acid (PAC) is also well known as a superabsorbent of water that can hold it even under pressure (Li et al., 2018; Tang et al., 2012). It is often used as the copolymer as it has the chemical structure which sufficiently expands the organic sub-phase of the copolymer electrolyte system. The organic sub-phase is very important in order to facilitate all transport mechanisms to increase the ionic conductivity of the electrolyte system (Lan et al., 2007; Stamenković et al., 1997).

To optimize the ionic dynamic motion, the host polymer PAAC doped with various ratios of sodium iodide (NaI) and the optimized PAAC-NaI solution mixture was further improved by adding various ratios of ionic liquid of 1-Butyl-3-Methylimidazolium Iodide (BMI). Propylene carbonate (PC) was added to the solution mixture as a plasticizer to fabricate flexible polymer electrolyte thin films (Selvasekarapandian et al., 2005).

1.2 Problems Statements

The challenging task in this research is to optimize the transport properties of solid polymer electrolytes, where the ion conduction mechanism is still not well known in solid polymer electrolytes. It is therefore essential to analyze the characteristics of the ion transport mechanism in polymer electrolytes along with the polymer segmental relaxation process. Furthermore, a thorough understanding of dielectric relaxation is a valuable tool for studying the in-depth ion transport mechanism and to carry out further research work about ion and molecular interactions in solid polymer electrolytes.

1.3 Aims and Objectives of Research

As mentioned earlier, PAAC (host polymer) doped with additive NaI (salt) and BMI (ionic liquid) with additive PC (filler) with high dielectric constant are the promising candidate of solid polymer electrolytes to investigate various methods to optimize the transport properties.

The main aim of this research is to understand the ion transport mechanism in ion conducting polymer electrolyte systems added with salt and optimized with ionic liquid. Especially, the research focusses on sodium salt conducting polymer electrolyte, where the recent development of the sodium ion batteries is largely motivated by its low cost, high abundance, and non-toxicity behavior.

In order to achieve the aims referred to the above, the following targeted objectives have been designed:

- To explore and measure the structural and electrical properties of the solid polymer electrolyte using X-Ray Diffraction (XRD) and Electrochemical Impedance Spectroscopy (EIS) characterization techniques.

- To examine and analyse the overall mechanism pertaining to ionic transport dynamics in the polymer electrolytes.
- To optimize the ionic conductivity at ambient temperature and measure the temperature dependent transport properties via dielectric and modulus electric spectroscopy methods.

1.4 Outline of Thesis

This thesis consists of five chapters. The first chapter is about the research background, aim/ motivation, and the research objectives. Solid polymer electrolytes (SPEs) based on copolymer Poly (acrylamide-co-acrylic acid) system with summarized background studies on the development of solid polymer electrolyte thin films comprised of copolymer, salt, additive, and ionic liquid systems.

Chapter two presents the detailed literature survey on overall conduction mechanism based on electrochemical impedance spectroscopy techniques including dielectric properties and electric modulus analysis. In this section, parameters of ionic conductivity, dielectric constant, dielectric loss, loss tangent spectra, ionic mobility, charge carrier density, and diffusion coefficient have all been investigated in relation to an appropriate ion transport model for polymer electrolytes.

Chapter three elaborates the detailed research methodology which not only outline the experiments and procedures to be carried out to prepare the sample but will also cover the characterization techniques involved in the study to analyze the samples.

In chapter four, the overall results of transport parameters are discussed comprehensively for System A and System B as follows:

- a) System A: Poly (acrylamide-co-acrylic acid) (PAAC) doped sodium iodide (NaI) at various ratios and added fixed amount of additive propylene carbonate (PC).

- b) System B: Optimized ratio of Poly (acrylamide-co-acrylic acid) (PAAC) and sodium iodide (NaI) and propylene carbonate (PC) added with 1-Butly-3-Methylimidazolium Iodide (BMI) with different ratios to identify the highest conductivity of the system.

Finally, in chapter five, the conclusions of the thesis presented includes the suggestions and recommendations for future research in this area of study especially to further optimize the transport properties, which are important for development of good quality solid polymer electrolytes for the variety of electrochemical devices.

Universiti Malaysia

CHAPTER 2: LITERATURE REVIEW

An overview of the literature on polymer electrolytes is presented in this chapter. The first section highlights the evolution of solid polymer electrolytes and provides an insight of the various types of solid polymer electrolytes. The second section describes the overall ionic conduction theory and reviews the parameters governing the transport properties of the polymer electrolytes and reveals the properties of temperature dependent ionic conductivity. The third section describes the methods of adding salt, ionic liquid and plasticizer to increase and optimize the ionic conductivity of polymer electrolytes and the fourth section discusses dielectric characteristics, including the impact of dielectric constant and dielectric loss on ionic conductivity and segmental relaxation process. The last fifth section explains the theory of diffusion model which helps to understand the nature of transport properties of the polymer electrolyte.

2.1 Solid Polymer Electrolytes

The first solvent-free polymer electrolyte complex with ionic salts was reported by Wright (Wright, 1975). Unfortunately, this solid polymer electrolyte is known to result in insufficient performance at ambient temperature, which acted as a barrier to its utility compared to the existing conventional liquid/hybrid electrolytes (Pradhan et al., 2008). Therefore, extensive research work was carried out to enhance its mechanical properties and ambient temperature ionic conductivity through blending with various other polymers, crosslinking agents (Wieczorek & Stevens, 1997), insertion of ceramic fillers (Przyłuski & Wieczorek, 1989), plasticization (Cherng, Munshi, 1987), and doping with ionic salts (Hassan & Arof, 2005). This information indicates that the utilization of doping salts which form low-temperature eutectics with polymers are a useful approach for obtaining a good flexibility of the polymeric chains which are responsible for the ionic transport in solid polymer electrolytes.

2.2 General Description of Ionic Conduction Mechanism

Ionic conductivity is one of the important key parameters that determines the performances of any electrochemical device. It is obvious that the main factors that control conductivity include the number of charge carriers and their mobility (Kaiser, 2001). This is applicable to all types of polymer electrolyte systems and the relationship can be described by equation 2.1:

$$\sigma = \sum_i^N n_i Z_i q \mu_i \quad (2.1)$$

Where n_i is the charge carrier density, q is the electron charge, μ_i is the ionic mobility and Z_i is the valence for the ionic species in the electrolyte system. It is clear that, the ionic conductivity (σ) increases when the charge carrier concentration, n_i and/or ionic species mobility, μ_i parameters increase in the system, as shown in the equation 2.1. (Gueye et al., 2020).

The ionic conduction mechanism in polymer complexes can be visualized by understanding the transitional move/hopping and dynamic segmental motion between coordinating sites, as well as local structural relaxations of the polymer chain within the host polymer. (Siva Kumar et al., 2006).

In general, there are three types of ionic conduction mechanisms developed by theoretical model based on cation transport modes. (Diddens et al., 2010):

- Cation diffusion mechanism along the polymer chain
- Cooperative motion of the cation within the polymer chain
- Transferring cations between the different polymer chains

2.2.1 Electrochemical Impedance Spectroscopy

A variety of techniques, including impedance spectroscopic methods, have been used to assess ion mobility under an applied electric field to better understand the details of the ionic conduction mechanism.

To assess the ion mobility, transient ionic direct current measurements have also been used in the last decade. This technique uses a DC voltage before the voltage is reversed after a steady state is reached and the current is measured as a function of time to assess mobility. Nuclear magnetic resonance, NMR, spectroscopy has also been utilized to analyze the behavior of ionic conductivity, but there are limited to polymer electrolytes and liquid electrolytes. Therefore, for all forms of ionic species, the NMR method cannot be employed (Hayamizu et al., 2002).

Despite several attempts, however, ion conduction mechanisms are still not well known for a decade of year in many systems and, in particular, ion mobility values are still problematic in some solid-state electrolyte systems. Therefore, a reliable and convenient method is required to evaluate the ionic conductivity mechanism (Klein et al., 2006).

Compared to several other methods, Electrochemical Impedance Spectroscopy (EIS) is a versatile and effective technique for studying the electrical properties of bulk materials and their interfaces (i.e., electrode-electrolyte interfaces) over a large alternating frequency range. This method is most successful experimental technique to measure the ion conductivity and dielectric relaxation in polymer electrolytes (Aziz et al., 2018).

The EIS offers several advantages, including the fact that during the experiment, a tiny perturbation of sinusoidal potential is applied throughout the cell or electrolyte, which

reduces the possibility of charge carrier concentration fluctuations. (Schütt & Gerdes, 1992).

In the EIS analysis, the applied alternating voltage (V) that varies with time (t), is defined as $V(t) = V_o \sin(\omega t)$ and resulting an alternating current (I) with phase angle (ϕ) is as follows; $I(t) = I_o \sin(\omega t + \phi)$

The impedance parameter, $Z(\omega)$ which is the direct ratio of the applied alternating voltage $V(t)$ and alternating current $I(t)$ which yields the complex impedance of Z_{real} and $Z_{imaginary}$ is as follows in equation 2.2:

$$Z^* = Z_{real} + jZ_{img} \quad (2.2)$$

$$Z_{real} = Z' = Z \cos \omega t \text{ and } Z_{img} = Z'' = Z \sin \omega t$$

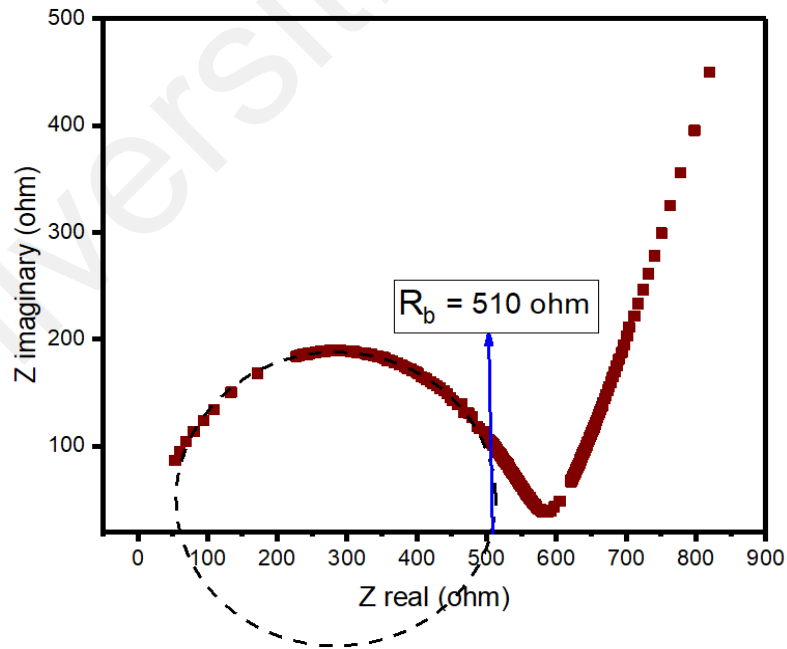


Figure 2.1: Impedance Plot of Z_{img} versus Z_{real} to exhibit bulk resistance R_b (Aziz et al., 2018).

The complex impedance data can be analyzed by using Cole-Cole plot of Z_{img} versus Z_{real} , which was used extensively by many researchers in the past few decades (Cole & Cole, 1941) where a semicircle is in high frequency region and a linear line is in the low frequency region (i.e., a spike) (Figure 2.1).

The bulk resistance R_b can be evaluated directly from the intercept of real axis of impedance plot from semicircle in high frequency region. In addition, as the phase angle reaches zero, the complex impedance is dominated by the DC conductivity (Wan et al., 2003). The low frequency spike has been attributed by the electrode blocking effect which is due to the effect of formation of hetero-charge layer accumulated near the electrode/electrolyte interface (Selvasekarapandian et al., 2005).

2.2.2 DC Conductivity and Temperature Dependent Conductivity

The DC conductivity deduced from the basic relationship of electricity flows through any conducting medium can be calculated from equation 2.3:

$$\sigma_{dc} = \frac{l}{R_b \times A} \quad (2.3)$$

Where l (cm) and A (cm²) are the thickness and cross-sectional area of the solid polymer electrolyte sample which is under investigation and R_b is the bulk resistance.

Overall, conductivity is seems to be increase as the degree of crystallinity decreases or, in other words, the polymeric backbone structural flexibility significantly increases as the salt and ionic liquid added to the polymeric system. Since PAAC is a polar polymer, it ionizes the NaI salt into anions and cations under the influence of applied electric field and temperature.

The Arrhenius-like relationship reported for the temperature dependent DC conductivity represents the fact that the motion of cations does not arise from the

molecular motion of polymer host (Carvalho et al., 2000). In this section, the relationship between the DC conductivity and temperature is explained in accordance with the well-known Arrhenius model, given by the equation 2.4:

$$\sigma = \sigma_o \exp(-E_a/kT) \quad (2.4)$$

Where σ_o is the pre-exponential factor, E_a is the activation energy, k is the Boltzmann constant and T is the absolute temperature in Kelvin.

As a result, as soon as the DC conductivity increases linearly with increase of temperature for all compositions of polymer complex and compatible with the Arrhenius relationship, the ionic transport properties can be associated with that which occurs within the crystalline polymer complex area where ions jump to the closest unoccupied sites, which enables a linear increase of DC conductivity. (Fattah et al., 2016).

When the temperature rises, the segmental vibrational energy is sufficient to push against the hydrostatic pressure exerted by the adjacent atoms and creating a small amount of space around its own volume in which vibrational motion can occur. At the same time, the polymer chain grows faster as the amorphous phase expands at high temperatures and when the bond rotation induces a segmental movement. This favors inter-chain and intra-chain ion hopping and enhance the ionic conductivity (Michael et al., 1997).

2.3 Methods to Enhance the Ionic Conduction Mechanism

2.3.1 Effects of Adding Salt, Ionic Liquids and Plasticizers

The sodium element (Na) in the ionic form found in the Sodium Iodide salt is extremely promising and has the ability to meet future energy demands. It is the sixth most plentiful element (found in 2.64 percent of the earth's crust) with low reduction potential (-2.7 V), low toxicity, softness, and low cost (seven times cheaper than lithium) that are the key strengths of sodium. Besides that, Sodium Iodide (NaI) added in System

A with various ratios which iodide salt acting as the effective charge carrier in the polymer electrolyte to improve the ionic conductivity. When sodium iodide salt is added to the electrolyte polymer, it starts to breakdown into free cation (I⁻) and anion (Na⁺) pair. In addition, the increased of pair charge carriers are able to generate free ion mobility more efficiently (Ling et al., 2020).

Various ratios of ionic liquid of 1-Butyl-3-Methylimidazolium Iodide (BMI) added in System B order to enhance further its ionic conductivity. Based on the findings, the ionic conductivity and the dielectric behaviors of the solid polymer complex improved upon incorporation ionic liquid until certain maximum ratio. The optimized conductivity-temperature plot revealed that the effectiveness transportation of ions in these films in System B obey Arrhenius theory (Chong et al., 2016).

Finally, plasticizer propylene carbonate (PC) of low molecular weight, high dielectric constant added to host polymer electrolyte system A and system B in a predetermined amount (Table 3.1 & 3.2) to improve mechanical strength flexibility, thermal stability, viscosity reduction, and improving by increasing the number of charge carriers (Sangeetha et al., 2017).

2.4 Dielectric Properties and Fundamental of Electric Modulus

In general, the study of complex dielectric permittivity ($\epsilon^*(\omega)$) is an essential method to probe and analyze the electrode polarization effect and understand the energy dissipation in terms of dielectric constant $\epsilon'(\omega)$ and dielectric loss $\epsilon''(\omega)$, respectively of ionic polymer electrolyte system. The definition for dielectric constant relates to the permittivity of the polymer electrolytes, $\epsilon'(\omega)$. The permittivity expresses the ability of a polymer electrolyte material to polarize in response to an applied field. It means the greater the polarization developed by a material in an applied field of given strength, greater is the dielectric constant. The permittivity of a polymer electrolyte expresses its

ability to polarize in response to an applied electric field. It means that greater the polarization effect created by a material in a given applied field, greater is the dielectric constant.

In the dielectric analysis, the interfacial polarization suppresses conductivity relaxation processes. Further analysis can be conducted using modulus spectroscopy which elucidates charge transport mechanisms such as the conductivity relaxation phenomena and ion dynamics as a function of frequency and temperature (Aziz, Brevik, et al., 2020).

2.4.1 Dielectric constant and Dielectric Loss

The dielectric constant $\varepsilon'(\omega)$ or the real part of electrical permittivity of the system represents the charges stored near the electrode-electrolyte interface in each cycle and dielectric loss $\varepsilon''(\omega)$ is the quantity that measure the energy losses due inability to polarize the ions quickly to follow the frequency of the oscillating electric field swiftly.

The dielectric constant and dielectric loss of the ion conducting polymer electrolyte system can be described by the real and imaginary part of the complex permittivity $\varepsilon^*(\omega)$ expressed in equation 2.5:

$$\varepsilon^* = \varepsilon'(\omega) - j\varepsilon''(\omega) = \frac{1}{j\omega C_o Z^*} \quad (2.5)$$

The real (ε') and imaginary part (ε'') of dielectric permittivity can be expressed in 2.6 and 2.7, respectively:

$$\varepsilon'(\omega) = \frac{Z''}{(Z'^2 + Z''^2)\omega C_o} \quad (2.6)$$

$$\varepsilon''(\omega) = \frac{Z'}{(Z'^2 + Z''^2)\omega C_o} \quad (2.7)$$

Where z' and z'' are the real and imaginary part of impedance, capacitance of free space defined as $C_o = \frac{\epsilon_o A}{d}$, ϵ_o is the permittivity of free space, d is the thickness of the solid polymer electrolyte film and A is the area of the blocking electrode and $\omega = 2\pi f$, ω is the angular frequency of the oscillating electric field.

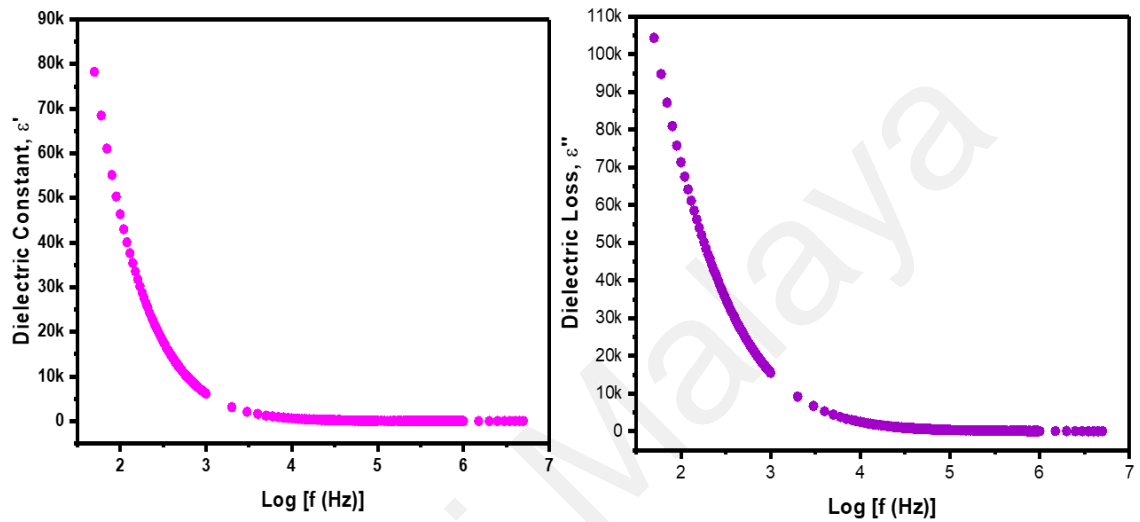


Figure 2.2: Dielectric Constant ϵ' and Dielectric Loss ϵ'' versus $\log f$ plot over broad range frequency (Sangeetha et al., 2021).

The variation of dielectric constant versus temperature is different for non-polar and polar polymers. For non-polar polymers, dielectric constant is generally independent of temperature. But in the case of polar polymers, the dielectric constant increases with the increase of temperature. Indeed, for polar polymers, there is a direct relationship between dielectric permittivity and temperature. The dielectric permittivity of non-polar polymers, on the other hand, is temperature independent. This is a property of polar dielectrics, in which the orientation of dipoles of the polar polymers will be induced and facilitated as temperature rises, resulting in an increase in dielectric permittivity. (Hougham et al., 1994). A clear comparison of dielectric constant and dielectric loss is shown in Figure 2.2. It can be observed that the dielectric loss values are greater than those of dielectric constant. This phenomenon can be explained through the fact that the orientation of

dipoles was facilitated with the rise in temperature and thus permittivity increased as well (Kumar et al., 2020).

2.4.2 Loss Tangent Spectra and Relaxation Time

The loss tangent defined from the above equations (2.4) and (2.5) as “the ratio of dielectric loss factor $\varepsilon''(\omega)$ to the dielectric constant $\varepsilon'(\omega)$ ” which can be derived using equation 2.8:

$$\tan\delta = \frac{\varepsilon''(\omega)}{\varepsilon'(\omega)} = \frac{Z'}{Z''} \quad (2.8)$$

The loss tangent is able to measure the ratio of the electrical energy lost to the energy stored periodically during oscillation of electric field. From these relationships, it can be concluded that dielectric loss $\varepsilon''(\omega)$ is exactly in proportion to the real part (Z' or R) of the impedance function, which is further elucidated through the equation 2.9:

$$\varepsilon''(\omega) = \frac{Z'}{(Z'^2 + Z''^2)\omega C_o} \quad (2.9)$$

In this study, the lost peak of $\tan \delta$ was analyzed to observe the relaxation behaviour in the polymer electrolytes. Relaxation behavior is a momentary delay as the charges and dipoles recover from their unperturbed state upon removal of AC stimulus. This is due to the segmental relaxation time (τ) occurs in a polymer chain, which is the time required for the dipoles to revert to their original random orientation. It does not happen instantly, but the polarization effect decreases exponentially.

The dielectric loss tangent ($\tan\delta$) as a function of frequency has been displayed in Figure 2.3 for better understanding the segmental relaxation process. The basic principles behind the plot shape of loss tangent ($\tan\delta$) can be interpreted in terms of Koops phenomenological principle (Koops, 1951). It is clearly seen that $\tan \delta$ increases with

frequency and reaches a maximum value at frequency f_{\max} , and thereafter decreases in high frequency region. The shortest relaxation time τ is recorded at the peak of the conductivity curve in Figure 2.3.

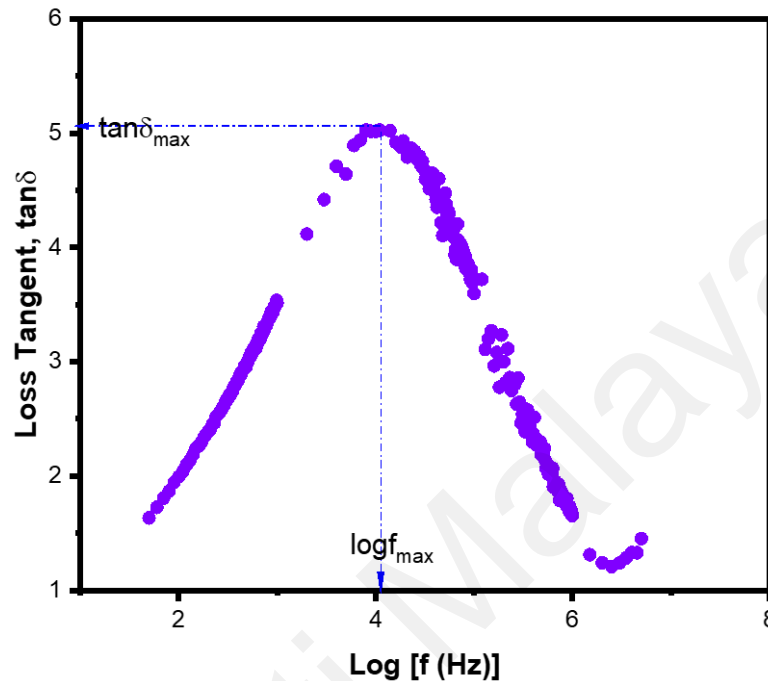


Figure 2.3 : Loss Tangent $\tan\delta$ versus $\log f$ plot over broad range frequency (Koops, 1951).

In the loss tangent analysis, the details of the capacitive and resistive components of the solid polymer electrolyte system can be explained from the shape of the $\tan\delta$ plot. The complex impedance relationship is $Z^* = R - jX_c$, where R is the real part of the impedance or resistor element and X_c is the capacitive element (Aziz et al., 2018). The imaginary part of the impedance ($X_c = 1/2\pi fC$), which the frequency dependent capacitive component's reactance reveals that at low frequencies, the reactance increases dramatically, and the majority of the current goes through the resistor element, where the ohmic component of the current increases more sharply than its capacitive component reactance.

On the other hand, at the higher frequencies, loss tangent ($\tan\delta$) decreases with increase in frequency because ohmic portion of the resistance is independent of frequency and the capacitive component of current increases as a consequence of the value of X_C which decreases to lower value at high frequency region (Louati et al., 2009).

2.4.3 Electric Modulus

Many researchers have used the electric modulus to examine and interpret electrical relaxation data in a wide range of materials. Transformation of dielectric spectra into electric modulus is an effective method to explore the behaviour of ionic conductivity relaxation mechanism to understand the electrode polarization effect (Świergiel & Jadżyn, 2011).

The electric modulus is the inverse of electric permittivity and can be described by equation 2.10 as the real and imaginary part of the complex permittivity $M^*(\omega)$:

$$M^*(\omega) = M'(\omega) - jM''(\omega) = \frac{1}{\varepsilon^*} = \frac{1}{\varepsilon'(\omega) - j\varepsilon''(\omega)}$$

$$M^*(\omega) = j\omega C_o Z^* = \omega C_o Z'' + j\omega C_o Z' \quad (2.10)$$

The real $M'(\omega)$ and imaginary part $M''(\omega)$ of electric modulus can be expressed further using equation 2.11 and 2.12:

$$M'(\omega) = \frac{\varepsilon'}{(\varepsilon'^2 + \varepsilon''^2)} \quad (2.11)$$

$$M''(\omega) = \frac{\varepsilon''}{(\varepsilon'^2 + \varepsilon''^2)} \quad (2.12)$$

In comparison with the pattern of dielectric loss $\varepsilon''(\omega)$ and dielectric constant $\varepsilon'(\omega)$, the real $M'(\omega)$ and imaginary part $M''(\omega)$ of electric modulus spectra demonstrate contrast

behaviour at low and high frequency region. Large values of dielectric spectra were observed at low frequency region compared to electric modulus spectra indicated the lowest values at low frequency region (Ramesh & Arof, 2001). The lowest values of electric modulus at the low frequencies, indicating the negligibility of electrode polarization effect, has been explored by Woo et al., and could be attributed to the suppression of low frequency electrodes/sample double layer effects, originating from the large capacitance established at the low frequency region (Woo et al., 2012). The peak in the $M''(\omega)$ spectra indicates the regions where the carrier ions can mobile along the long distance (left of the peak) or where the carrier is confined (right of the peak) (Mohd Faiz Hassan & Yusof, 2014) (Figure 2.4).

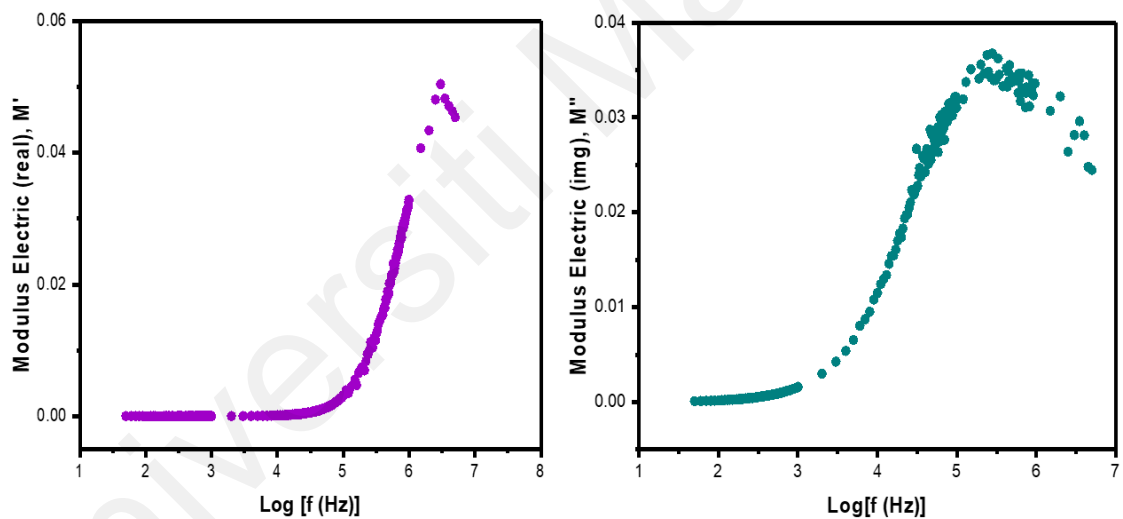


Figure 2.4: Modulus electric real M' and Modulus electric imaginary M'' versus log f plot over broad range frequency (Woo et al., 2012).

However, by comparing the behaviour of the asymmetric peak of the $M''(\omega)$ agrees with the non-exponential behavior of the conductivity relaxation, which can be described by the Kohlrausch-Williams-Watts function (Williams & Watts, 1970), $\varphi(t) = \varphi_0; (0 < \beta < 1)$, where τ_∞ and β are the conductivity relaxation time and Kohlrausch exponent respectively.

The β parameter (corresponding to all the composition) has been estimated using the formula $\beta=1.14/\text{FWHM}$. Where the full width at half maximum (FWHM) of the modulus peak displaying the stretched exponential function that reveals the non-Debye behaviour of the materials which corresponds to long-time slow polarization and relaxation of hopping charge carriers.

2.5 Transport Properties and Diffusion Model for Ionic Conductivity

The ionic transport properties mainly depend on the degree of salt dissociation and its concentration, dielectric constant, degree of ion aggregation, and the mobility of polymer chains.

2.5.1 Transport Model Analysis

By evaluating the peak value of loss tangent graph (Figure 2.3), the transport parameters of charge carrier density, mobility, and diffusion coefficient were determined using the Trukhan model (Munar et al., 2011). The diffusion coefficients of cations and anions are considered to be identical in this model, hence the diffusion coefficient was calculated using a simple expression from the peak value in the loss tangent plots. The expression of the Trukhan model is given in equation 2.13:

$$D = \frac{2\pi f_{max} L^2}{32(\tan^3 \delta)_{max}} \quad (2.13)$$

where L is the sample thickness, f_{max} is the frequency at loss tangent peak value which can be directly calculated from loss tangent graph depicted in Figure 2.3.

Another key metric in relation to conductivity, the ionic mobility (μ), which may be calculated using the well-known Nernst-Einstein relation and the Trukhan model for diffusion coefficient given in equation 2.14:

$$\mu = \frac{eD}{k_B T} = \left(\frac{e}{k_B T} \right) \left[\frac{2\pi f_{max} L^2}{32(\tan^3 \delta)_{max}} \right] \quad (2.14)$$

The charge carrier density (n) is also another parameter that can be calculated from the following conductivity and mobility relations and the Trukhan model given in equation 2.15:

$$\begin{aligned} \mu &= \frac{\sigma_{DC}}{ne} \quad \text{and} \quad \mu = \frac{eD}{k_B T} \\ n &= \frac{\sigma_{DC} k_B T}{e^2 D} \\ n &= \left(\frac{\sigma_{DC} k_B T}{e^2} \right) \left[\frac{32(\tan^3 \delta)_{max}}{2\pi f_{max} L^2} \right] \end{aligned} \quad (2.15)$$

Based on above relationship, the carrier density, n is almost constant if the $(\tan^3 \delta)_{max}$ do not change significantly as the temperature changes.

2.5.2 Relationship between carrier charge density (n), ionic mobility (μ) and diffusion coefficient (D)

The frequency corresponding to the maximum value of $(\tan \delta)_{max}$ can be fitted into Arrhenius equation as follows; $f_{max} = f_o e^{(-E_m/kT)}$, where f_{max} is the frequency at relaxation peak, f_o is the constant and E_m is the ion migration energy at certain absolute temperature (Ravi et al., 2011).

The expression for the temperature dependent diffusion coefficient can be derived based on the Arrhenius relationship given in equation 2.16:

$$D = \frac{2\pi f_{max} L^2}{32(\tan^3 \delta)_{max}} \quad \& \quad f_{max} = f_o e^{(-E_m/kT)}$$

$$D = \left[\frac{2\pi L^2}{32(\tan^3 \delta)_{max}} \right] f_o e^{(-E_m/kT)}$$

$$D = D_o e^{(-E_m/kT)}; \text{ where } D_o = \frac{2\pi f_o L^2}{32(\tan^3 \delta)_{max}} \quad (2.16)$$

The temperature dependent ionic mobility can be derived further as given in equation 2.17:

$$\mu = \frac{eD}{k_B T} \quad \& \quad D = D_o e^{(-E_m/kT)}$$

$$\mu = \frac{eD_o e^{(-E_m/kT)}}{k_B T}$$

$$\mu = \mu_o(T) e^{(-E_m/kT)}; \text{ where } \mu_o(T) = \frac{eD_o}{k_B T} \quad (2.17)$$

From the above expressions for the temperature dependent diffusion coefficient and ionic mobility, it is found that both transport parameters exhibit the direct relationship between each other.

CHAPTER 3: METHODOLOGY

This chapter consists of three main sections. In the first section, chemicals used for the preparation of the sodium iodide based solid polymer electrolytes are described. The second part is about the detailed explanation of sample preparations of two types of solid polymer electrolyte which comprises of System A: Poly (acrylamide-co-acrylic acid) (PAAC) incorporated with sodium iodide (NaI) and System B: Poly (acrylamide-co-acrylic acid) (PAAC) incorporated with sodium iodide (NaI) optimized with 1-Butly-3-Methylimidazolium Iodide (BMI). The last part of the experimental work describes the characterization techniques to identify the structural and morphology of the above stated polymer electrolyte samples and also to analyze the electrochemical impedance properties of both system A and system B.

3.1 Materials and Sample Preparation

Generally, the solid polymer thin film membranes were prepared using a single solvent by the solution casting technique (Figure 3.1). The details of the compositions of the system A are PAAC (Aldrich, average molecular weight $\sim 5 \times 10^6$ powder) doped with NaI (Sigma-Aldrich, 99.99%) and a fixed amount of propylene carbonate (PC) was added to the mixture of the solution as per listed in Table 3.1. The fixed amount of PC was added to provide more flexibility to the polymer film by increasing the plasticity of the thin film membrane, where the PC has a low molecular weight and a high dielectric constant, which improves mechanical strength, thermal stability, and ionic conductivity overall.

Table 3.1: The Compositions of the System A: PAAC-NaI polymer electrolyte

| System A | PAAC (g) | NaI (g) | PC (g) | Total (g) |
|-----------------|-----------------|----------------|---------------|------------------|
| N10 | 0.80 | 0.10 | 0.10 | 1.00 |
| N20 | 0.70 | 0.20 | 0.10 | 1.00 |
| N30 | 0.60 | 0.30 | 0.10 | 1.00 |
| N35 | 0.55 | 0.35 | 0.10 | 1.00 |
| N40 | 0.50 | 0.40 | 0.10 | 1.00 |

In System B, the polymer thin film membrane samples were prepared by using the same solution casting technique. The solution of N30 compositions of the PAAC doped with sodium iodide (NaI) and fixed amount of propylene carbonate (PC) optimized by adding ionic liquid of 1-Butyl-3-Methylimidazolium Iodide (BMI) as per listed in Table 3.2.

Table 3.2: The Compositions of the System B: PAAC - NaI - BMI polymer electrolyte

| System B | BMI (g) | PAAC (g) | NaI (g) | PC (g) | Total (g) |
|-----------------|----------------|-----------------|----------------|---------------|------------------|
| BMI 10 | 0.100 | 0.540 | 0.270 | 0.090 | 1.000 |
| BMI 15 | 0.150 | 0.510 | 0.255 | 0.085 | 1.000 |
| BMI 20 | 0.200 | 0.480 | 0.240 | 0.080 | 1.000 |
| BMI 25 | 0.250 | 0.450 | 0.225 | 0.075 | 1.000 |

For both System A & System B, the mixture of each sample was stirred continuously with a magnetic stirrer for 24 hours at room temperature to obtain the homogenous solution. The solutions were then casted in glass Petri dishes, and the samples were dried at 60 °C in oven. After 24 hours, mechanically strong, transparent, and free-standing films

were obtained (Figure 3.2) and peeled off for the physico-chemical characterization and transport property studies (Figure 3.3).



Figure 3.1: (a), (b) and (c) System A [PAAC-NaI] solutions stir uniformly with magnetic stirrer and the casted solution after stir 24 hours respectively.

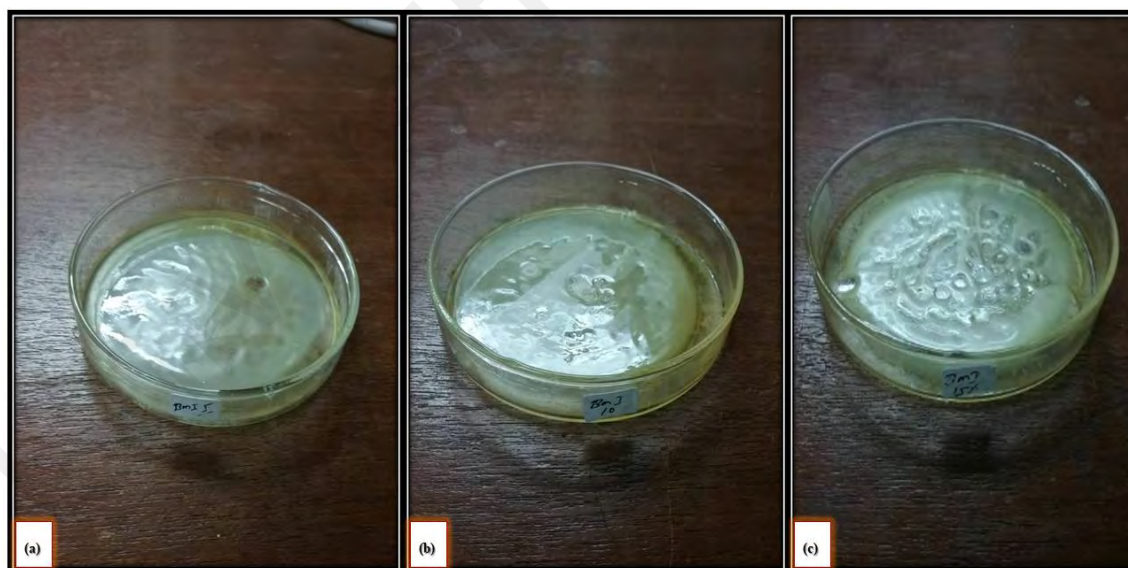


Figure 3.2: Free standing solid film after dried in oven at 60 °C for System B.

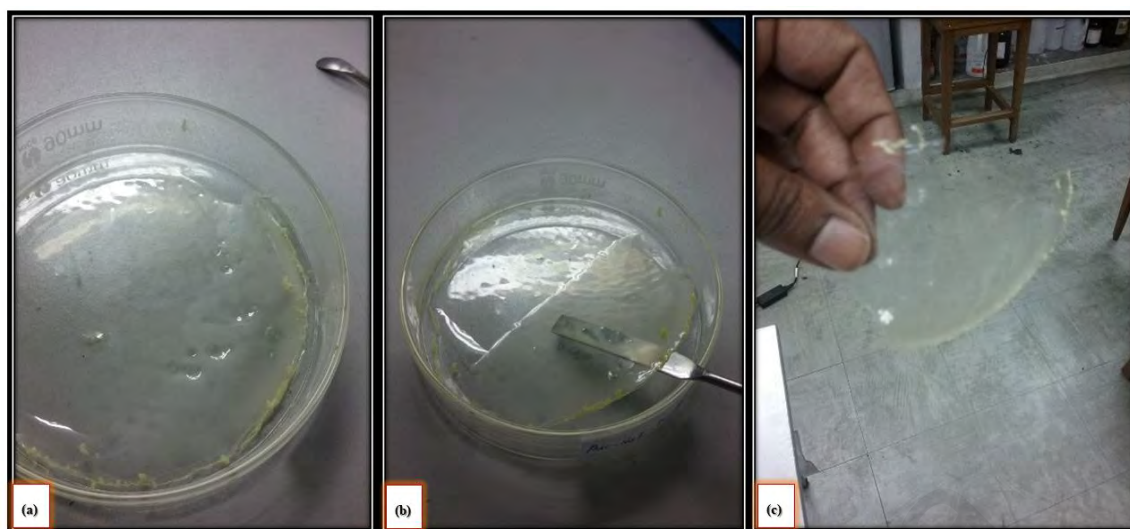


Figure 3.3: The clear and transparent solid electrolyte film peel off from petri dish.

3.2 Characterization

3.2.1 X-Ray Diffraction Analysis

X-ray diffraction presents the dual (particles/ waves) nature of X- rays which is used to attain information regarding crystallinity of the material. This technique is mainly used to identify and characterize the materials based on the diffraction pattern. However, it does not provide information about chemical composition of the testing material. The samples' crystallinity in this work was determined via X-Ray diffraction (XRD; D5000, Siemens) where samples were exposed to an accelerating voltage of 40 kV and current of 30 mA using Cu K α radiation (1.5406 Å) at a scan rate of 1° min⁻¹. The diffraction angle was varied from 5-55° at 2 θ at a temperature of 25 °C.

3.3 Electrochemical Impedance Spectroscopy (EIS) Analysis

The electrochemical impedance spectroscopy (EIS) was used to probe the overall conductivity and to investigate the ion transport mechanism, complex impedance spectroscopy and temperature dependent DC conductivity measurements. EIS study was performed on stainless steel two blocking electrodes configuration. The prepared samples

were cut in to 2 cm diameter size and placed between two stainless steel blocking electrodes of the sample holder as shown in Figure 3.4.

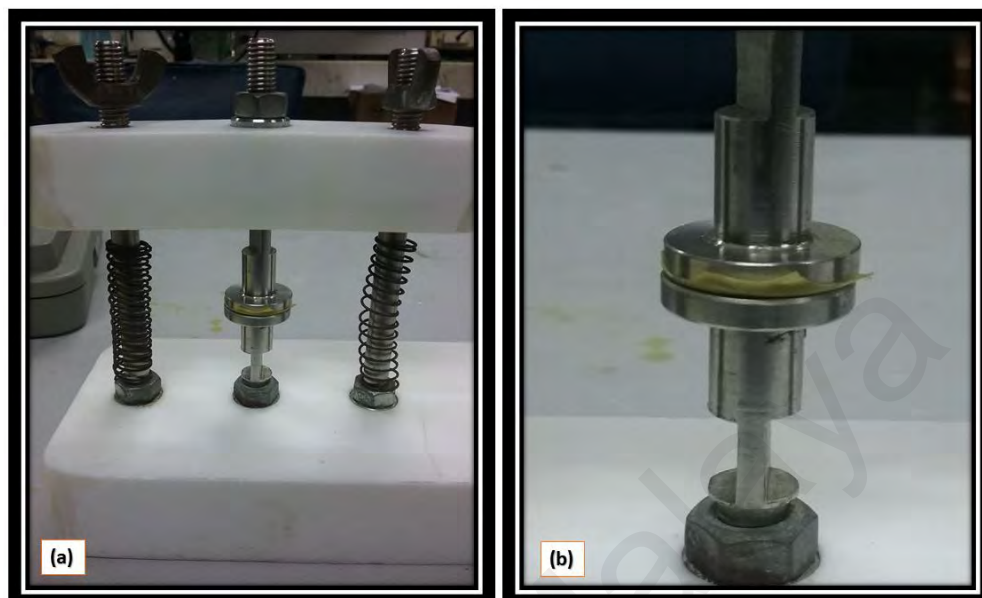


Figure 3.4: (a) The two-electrode parallel blocking stainless steel electrodes plate configuration system & (b) The prepared samples sandwiched between the sample holders.

The ionic conductivity was measured using HIOKI 3532-02 LCR Hi-Tester which was interfaced to the computer and the complex impedance spectroscopy Z_{img} versus Z_{real} of the polymer thin film membrane measured over the frequency range from 50 Hz to 5,000,000 Hz. The experiment was performed at room temperature and repeated for the interval of 10 °C up to 100 °C to analyze the temperature dependent electrochemical impedance properties.

CHAPTER 4: RESULTS AND DISCUSSION

This chapter has been divided into five main sections. The results and discussion based on system A: PAAC-NaI and optimized system B: PAAC-NaI-BMI has been described. In the first section, DC ionic conductivity was observed based on impedance data yields from electrochemical impedance spectroscopy of the system A and the second section reveals the optimized DC conductivity of the system B. In the third and fourth sections, the broadband dielectric characterizations including electric modulus of both System A and System B respectively are discussed. In the fifth and final part of this chapter, brief transport parameters of diffusion coefficient and ionic mobility results of system A and system B are compared to evaluate the factors playing key role to optimize the transport properties of the solid polymer electrolytes.

4.1 Characterization

4.1.1 Structural Characterization (X-Ray Diffraction Analysis)

XRD analysis was conducted to investigate the structural and phase studies of all the fabricated solid polymer electrolyte thin films containing different contents of sodium iodide. The XRD patterns of pure sodium iodide is demonstrated in Figure 4.1 (a) and the patterns of solid polymer electrolyte thin films are shown in Figure 4.1 (b). Sodium iodide reveals the sharp crystalline peaks at 17.5° , 19° , 22° , 23° , 27° , 29° , 33° , 36° , and 47° owing to the crystalline nature. The JCPDS numbers have been identified and included in the figure (Tan et al., 2020). However, solid polymer electrolyte thin films exhibited one broad peak around 20° - 23° which is evidence for the amorphous nature of the solid polymer electrolyte thin films even in the presence of purely crystalline sodium iodide salt having numerous sharp peaks at 2θ . All the sodium iodide peaks disappeared in the solid polymer electrolytes because of the complete dissociation of salt. The amorphous hump shows a minimal shifting in position with the addition of salt, which indicates that

the polymer has become more flexible (amorphous) with the availability of more vacant sites for the ease of ion transport through the polymer backbone. This ion hopping enhances the overall ionic conductivity. These amorphous humps could be assigned to a long-range chain order due to the strong polar intra- and intermolecular interactions. With the incorporation of sodium iodide up to 30 wt.% (N30), the diffraction peaks broaden which indicates a decrease in crystallinity of solid polymer electrolyte. This increase in the amorphous nature is due to the breakage of cohesive forces between the polymer chains from the salt. As a result, there is more available free volume to enhance the segmental motion and higher charge carrier mobility (Jingwei Wang et al., 2020). However, a further increase in the salt content again causes an increase in the crystallinity (N35). Thus, it is concluded that the ionic conductivity increases with a decrease in crystalline nature due to reduction in energy barrier. The ionic conductivity of the polymer electrolytes has an inverse relation with the crystallinity of the samples (Ahmad et al., 2011).

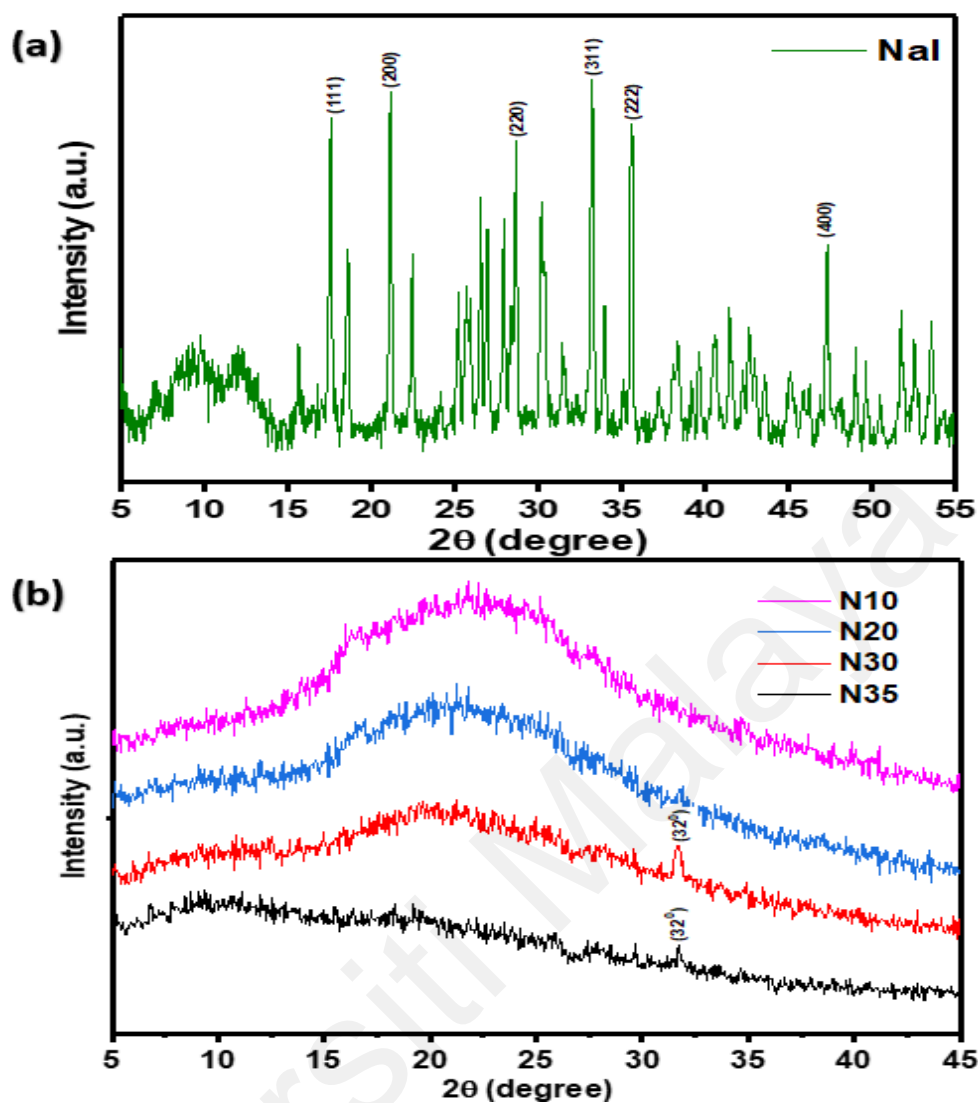


Figure 4.1: X-Ray diffractogram of (a) sodium iodide and (b) solid polymer electrolyte thin films.

4.2 Ionic Conductivity and Activation Energy

In this section, the ionic conductivity and the activation energy were used to compare the performance and electrical properties of both system A and system B by means of impedance plots at different temperatures. The ionic conductivity (σ) of the polymer electrolytes were calculated by using the equation 2.3. The highest ionic conductivity at ambient temperature was found to be $1.88 \times 10^{-5} \text{ Scm}^{-1}$ for the 30 % NaI-doped polymer electrolyte for system A with the lowest activation energy of 0.48 eV as shown in Figure 4.2. On the other hand, the conductivity increased up to maximum value of $4.73 \times 10^{-4} \text{ Scm}^{-1}$ and lowest activation energy of 0.26 eV for the optimized system B containing

15% ionic liquid BMI. The ionic conductivity and activation energy of System B are expressed in Figure 4.3.

The enhancement in ionic conductivity of the developed polymer electrolytes can be explained by physical interactions between polymeric chain and salt, especially the transition from a semi crystalline phase to an amorphous phase of the polymer complexes due to the dispersion of NaI. The increase of NaI salt increases the segmental mobility of polymeric chain until a maximum salt concentration and the ionic mobility decreases further due to higher salt concentration, where the ion pairs aggregate to form ionic clusters. These ionic clusters are less mobile and can promote the formation of crosslinking and stiffening of the polymeric matrix.

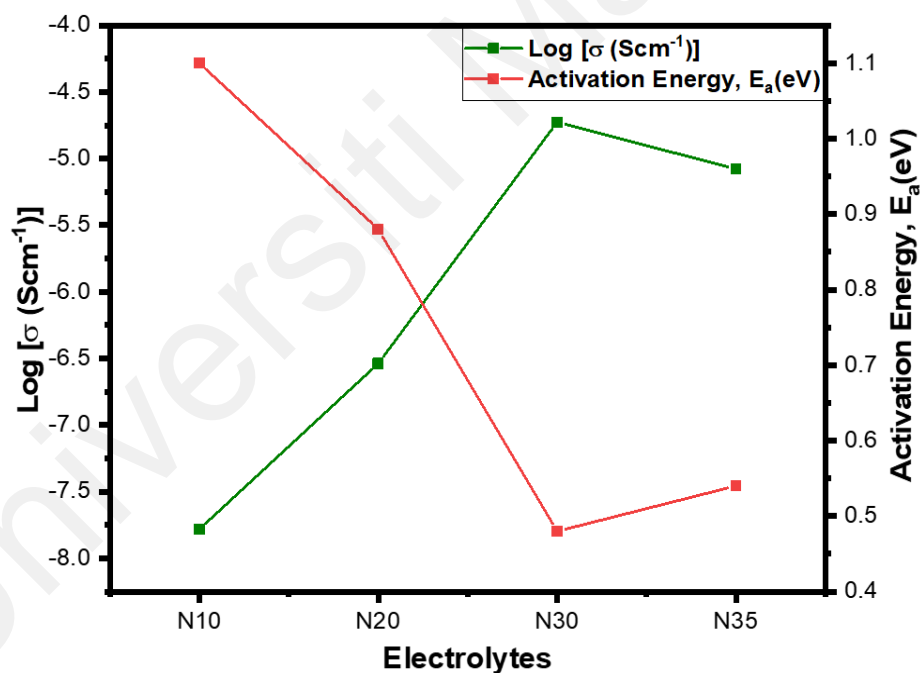


Figure 4.2: Log (conductivity) and activation energy plots of different [PAAC-NaI] electrolyte system.

The ionic conductivities of the PAAC-NaI polymer electrolyte systems with different concentrations of salt at room temperature are given in Figure 4.2. It has been observed that the ionic conductivity increases with the increase in concentration of salt up to 30% followed by significant decrease in ionic conductivity at higher concentrations. The

increase in conductivity with increasing salt concentration was due to increase in the number of mobile charge carriers and increase in the amorphous nature of the polymer electrolyte. On the other hand, the decrease in conductivity was observed for composition of 35% of salt. This was due to the aggregation of ions, leading to a decrease in the number of mobile charge carriers per unit volume leading to decrease in the mobility of ions (Nithya et al., 2014). Additionally, decrease of free volume in polymer matrix due to accumulation of the NaI salt can make conformational changes of the polymer chains leading to the hindrance of insertion/de-insertion of ions on polymer electrolyte surface (Jingping Wang et al., 2014). Therefore, the decrease in the ionic conductivity can be correlated with decrease of free volume as the salt concentration exceeded from 30%.

The energy needed by ion clouds to overcome the barrier to move freely is activation energy. The lower the activation energy, the higher the conductivity, as more electrons and ions are excited, and the current increases because of the higher electron mobility. From the Figure 4.2, the activation energy decreases with increase in salt concentration until 30%. This indicates the increase in amorphous nature of the polymer electrolyte membrane with addition of salt that eases the ionic transport mobility in the polymer network, where the polymeric chain in the amorphous nature becomes more flexible due to which the segmental motion of the host polymer increases (Zhang et al., 2007).

Similarly, the ionic conductivity increased upon adding ionic liquid BMI. This increase was observed until 15 wt.% ionic liquid and then started decreasing. It is owing to the aggregation of ionic liquid which hindered the ions mobility. The results are shown in Figure 4.3.

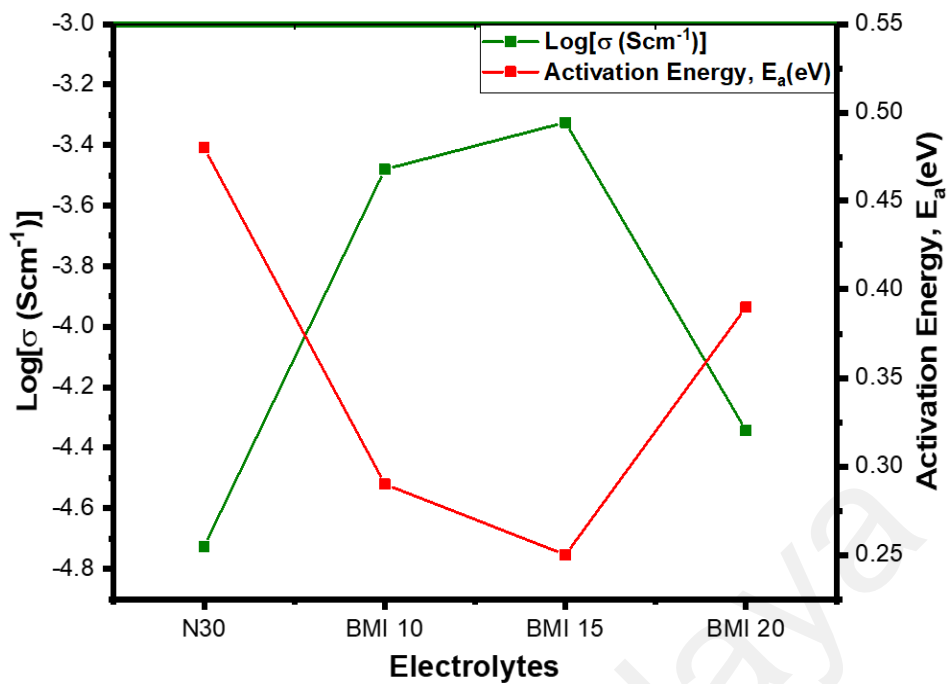


Figure 4.3: Log (conductivity) and activation energy plots of different [PAAC-NaI-BMI] electrolyte system.

4.2.1 Temperature Dependence Arrhenius behavior of Ionic Conductivity

The characteristic advantage of choosing solid polymer electrolytes in a specific electrochemical system application is practically based on the DC conductivity value. The relationship between DC conductivity and temperature in accordance with the well-known Arrhenius model is explained in this section and results are demonstrated in Figure 4.4.

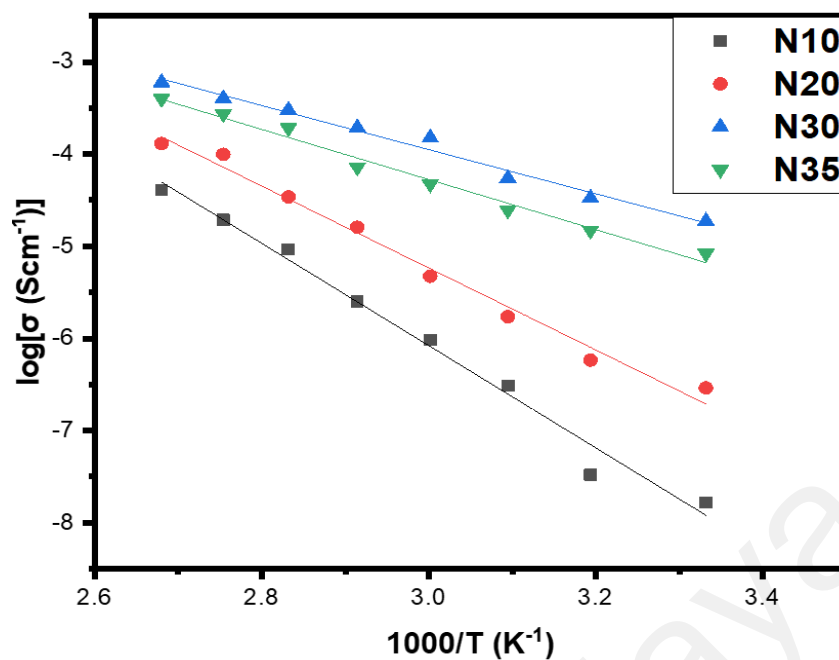


Figure 4.4: Temperature dependent ionic conductivity of different [PAAC-NaI] electrolyte system A.

The characteristic of Figure 4.4 represents the temperature dependent ionic conductivity of PAAC:NaI polymer electrolyte systems with different concentrations of the NaI salt. It has been observed that when the temperature was increased, the bulk resistance R_b was decreased which led to increase in ionic conductivity due to the ionic transport mechanism of solid polymer electrolytes. In fact, when the temperature was increased, the ionic mobility of the polymer chain was enhanced and the fraction of free volume in a solid polymer electrolyte was also increased accordingly, which led to an increase in ionic conductivity of polymer electrolyte (Zhu et al., 2001).

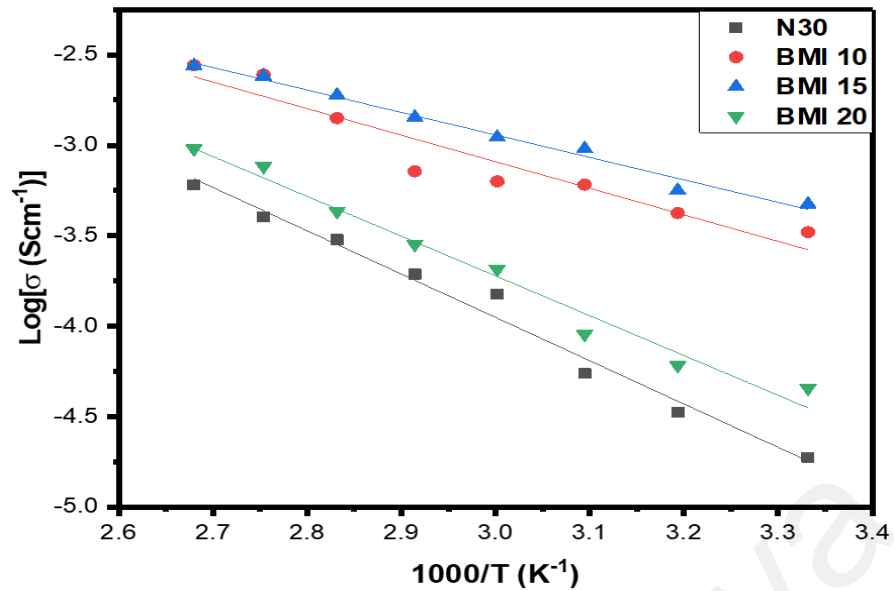


Figure 4.5: Temperature dependent ionic conductivity of different [PAAC-NaI-BMI] electrolyte system B.

It has been observed that the conductivity increases linearly with increase of temperature for all compositions of ionic liquid containing polymer electrolytes. Where the DC conductivity values follow the Arrhenius type thermally activated process (Fattah et al., 2016). The activation energy for all the prepared polymer electrolytes was calculated by linear fit of the Arrhenius plot using equation: $\sigma_{dc}(T) = \sigma_o \exp\left(\frac{-E_a}{k_B T}\right)$; where σ_o is the pre-exponential factor, E_a is the activation energy, and k_B is the Boltzmann constant.

The Arrhenius relationship as indicated by Figure 4.4 and Figure 4.5, shows that DC conductivity of cation motion is not solely due to the segmental motion of the polymer host. As a result, temperature and ionic conductivity data closely follow the Arrhenius relationship, and the cation transport mechanism can be correlated to ionic hopping mechanism to the nearest vacant site, allowing DC ionic conductivity increases as the temperature increases.

The ion hopping process mainly governs the mobility of ions in this system. Some of the electrons in the electrolyte gain energy and become free electrons when the temperature rises, promoting conduction. When the temperature of electrolytic solutions is raised, the viscosity of the solution decreases and the mobility of the ions in the solution increases.

4.3 The Broadband Dielectric Spectroscopy Analysis

The definition for dielectric constant relates to the permittivity of the polymer electrolytes, $\epsilon'(\omega)$. The permittivity expresses the ability of a material to polarize in response to an applied field. The dielectric constant or the real part of electrical permittivity of the system represents the charges stored in each cycle. It's actually the ratio of the dielectric permittivity to the permittivity of a vacuum. It means that the more the polarized ionic cloud induced by the applied electric field, the higher the dielectric constant. Study of complex dielectric permittivity (ϵ^*) is an important tool for understanding the electrode polarization effect and energy dissipation in terms of dielectric constant ϵ' and dielectric loss ϵ'' , respectively of ion conducting polymer electrolyte materials.

The broadband dielectric spectroscopy analysis of the System A composed of PAAC: NaI electrolytes were analyzed in view of the dielectric permittivity and dielectric modulus of the electrolytes. In principle, during the EIS experiment, an AC electric signal is applied to the polymer thin film and the corresponding impedance response of polymer electrolyte thin film is plotted in its rectangular form (with real and imaginary impedance). Basically, the dielectric studies revealed that the transport mechanism of NaI salt ions through the PAAC polymer chain electrolytes was mainly due to ion hopping mechanism coupled with the segmental motion of the polymer chain (Chong et al., 2017).

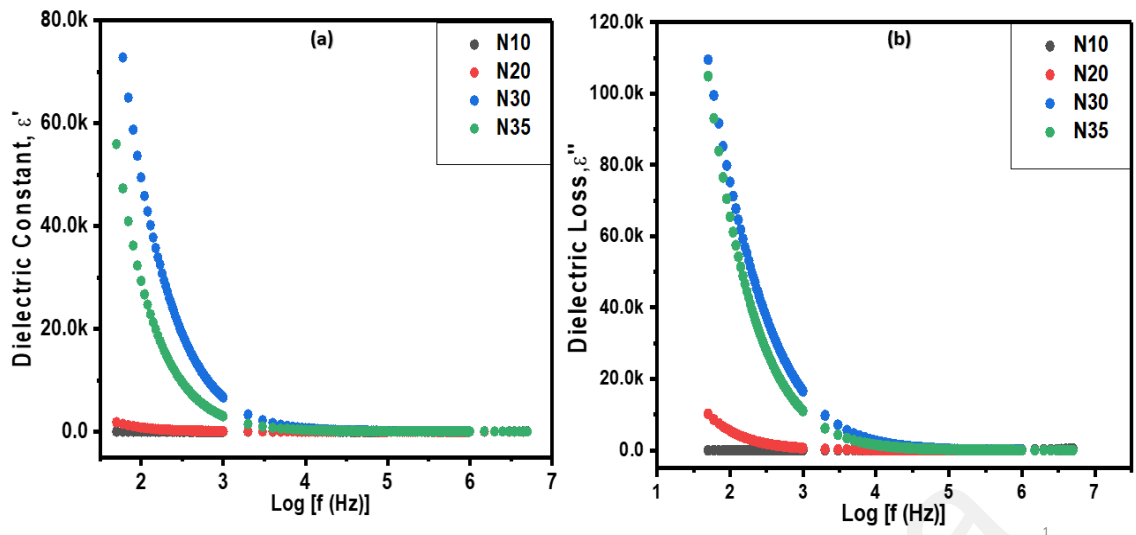


Figure 4.6: The (a) ϵ' versus $\log f$ and (b) ϵ'' versus $\log f$, plots of different [PAAC-NaI] electrolyte system A at room temperature.

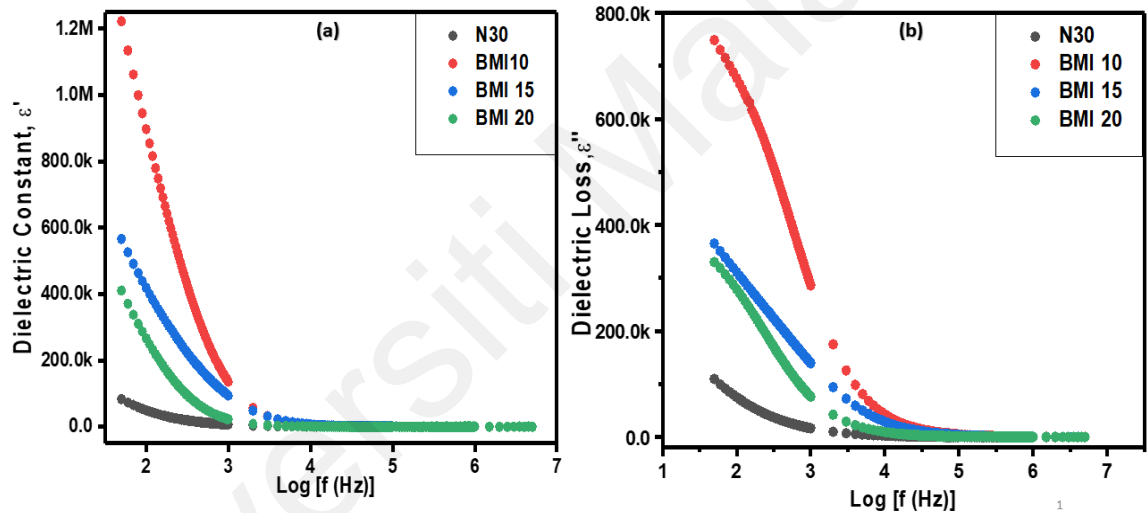


Figure 4.7: The (a) ϵ' versus $\log f$ and (b) ϵ'' versus $\log f$, plots of different [PAAC-NaI -BMI] electrolyte system B at room temperature.

It is clear from the Figure 4.6 (a) and Figure 4.7(a), for both System A and System B, the values of dielectric constant ϵ' are very high at low frequency region that means ϵ' increased rapidly by polarization effect due to the accumulation of charge carriers near the blocking electrodes (Campbell et al., 2001; Kim, 2001; Mishra & Rao, 1998). This will lead to increase in the storage of the dipole electric charges per unit volume at low frequency region. As the frequency of applied alternating electric field was increased, the dielectric constant ϵ' decreased and became constant at higher frequency region. At this

higher frequency region, the periodic reversal of electric field occurs at fastest rate until there is no excess ion diffusion in the direction of the field (Macdonald JR, 1992).

With increased frequency, there was almost no time for charge accumulation at the interface, but only for build-up charges at the boundaries of conducting species in the material and at the ends of conducting channels. The variation of the dielectric loss ϵ'' with $\log f$ exhibited in Figure 4.6 (b) and Figure 4.7 (b) clearly indicates the energy losses as the polarity of AC electric field reverses which causes the ion translational diffusion and dipole orientation undergoes deceleration and acceleration in the reverse directions. This reverse polarization creates heating effect through internal friction and causes the dielectric loss dissipated as the heat energy (Macdonald JR, 1992).

The dielectric losses increased with the addition of salt content, as the increased density of charge carriers underwent internal friction and generated huge amount of heat energy dissipation until 30% of the NaI salt concentration (Figure 4.6 (b)). Dielectric loss was then reduced for the salt concentration more than 30% due to re-association of the ion clusters.

4.3.1 Temperature Dependent Dielectric Spectra

Both of the dielectric constant and dielectric loss increase non-linearly with rising temperature, especially at low frequency region, according to a temperature-dependent dielectric study. Based on the analysis made from Figures 4.8 and 4.9, the overall dielectric ϵ' and dielectric loss ϵ'' always exhibit high values as the temperature increased. The high values of ϵ' and ϵ'' may be correlated to the interfacial structure at the bulk and the electrode region of the sample. From these figures, it is seen that both dielectric constant and dielectric loss decrease with increasing frequency but increase with increasing temperature (Singh et al., 2020). At all temperatures, high values of ϵ' and ϵ''

were observed at low frequencies, but at higher temperatures and frequencies, ϵ' and ϵ'' became relatively constant (Kumar et al., 2020).

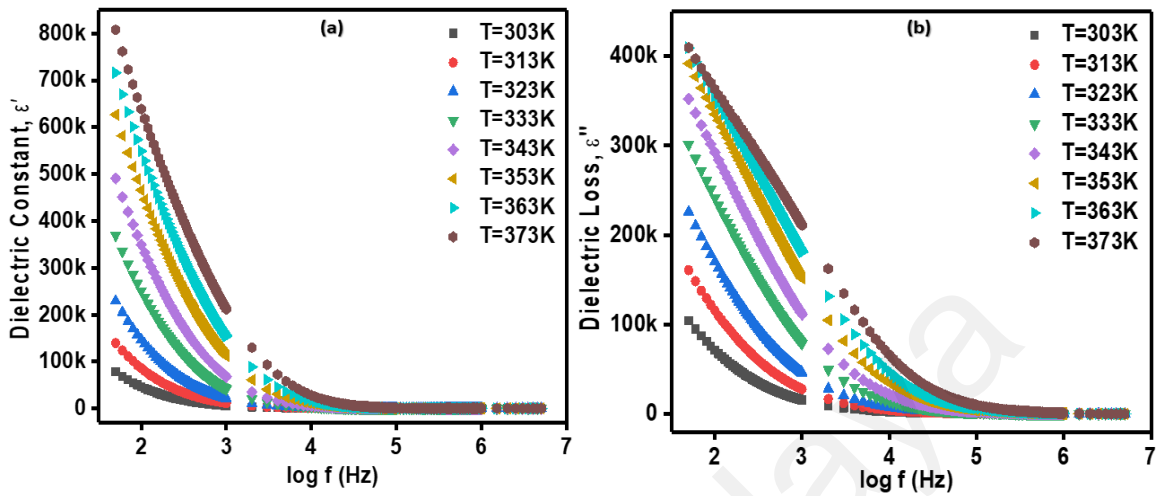


Figure 4.8: The temperature dependent (a) ϵ' versus $\log f$ and (b) ϵ'' versus $\log f$ respectively for optimized N30 electrolyte system A.

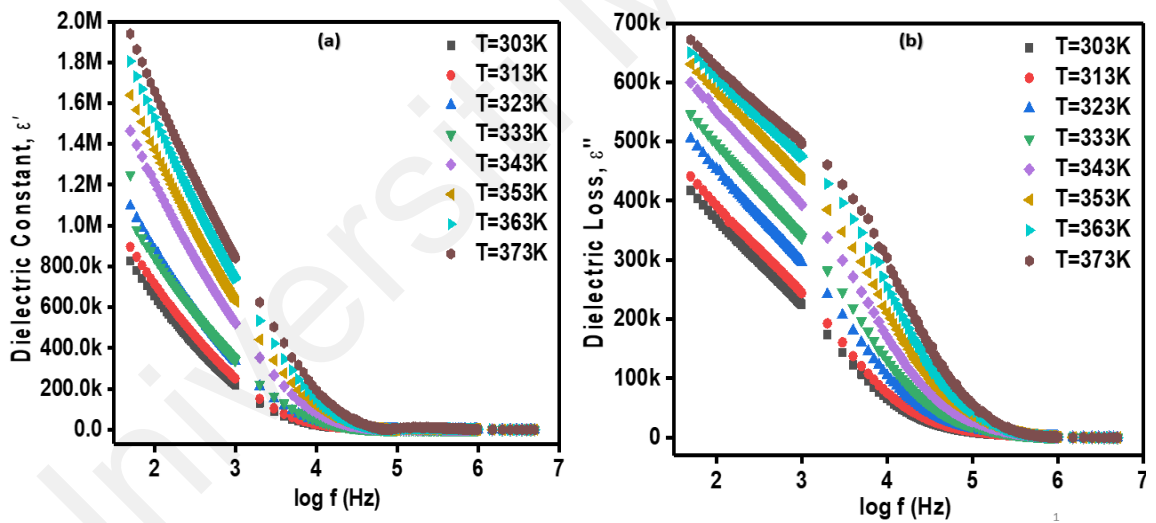


Figure 4.9: The temperature dependent (a) ϵ' versus $\log f$ and (b) ϵ'' versus $\log f$ respectively for optimized BMI15 electrolyte system B.

By comparing Figure 4.8 (a) and Figure 4.9 (a), the frequency dependent dielectric constant and dielectric loss were recorded for the highest values for the optimized System B (BMI15) at high frequency region. It indicates, there is strong correlation between the ionic conductivity and dielectric constant. According to most of research findings, the charge carrier density, n is primarily determined by the dissociation energy (U) and

dielectric constant (ϵ') of the polymer electrolyte, as represented in equation 4.1 (Awadhia & Agrawal, 2007):

$$n = n_o \exp\left(-\frac{U}{\epsilon' k_B T}\right) \quad (4.1)$$

The relationship highlights the strong correlation between dielectric constant (ϵ') and the density of charge carriers. Indeed, there is an increase of dielectric constant directly related to the increase of charge concentrations in the electrolyte as mentioned in equation (4.1). Therefore ionic conductivity (σ) depends upon both the number of charge carriers (n) and the mobility of the ionic species in the system as highlighted by equation (2.1). The increase in the value of dielectric constant with optimized salt concentration at N30 and optimized ionic liquid concentration at BMI 15 indicates that there is an increase in charge carrier concentration and hence an increase in DC conductivity as well (Dhatarwal & Sengwa, 2020).

4.3.2 Tangent Loss Spectra Analysis at room temperature

The variation of the loss tangent as a function A.C. frequency for the System A: PAAC incorporated with different concentrations of the NaI salt and the optimized System B: with various ratios of BMI are presented in Figure 4.10 (a) and Figure 4.10 (b), respectively. The loss tangent also consists of well-defined peak characteristics frequency, f_m . For System A and System B, it is clearly seen that $\tan \delta$ increased with frequency and reached a maximum value at frequency f_m , and thereafter decreased in high frequency region. At low frequency region, $\tan \delta$ increased with increase in frequency as the ohmic resistance was more dominant than reactance component for capacitance of the dipole charges. At the higher frequency region (MHz), $\tan \delta$ decreased with increase in frequency because ohmic portion is independent of frequency and the reactance component decrease with frequency (Chopra et al., 2003). In this study, the lost peak of

$\tan \delta$ was analyzed to observe the relaxation behaviour in the polymer electrolytes. Relaxation behaviour is a momentary delay as the charges and dipoles recover from their unperturbed state upon removal of AC stimulus. The shortest relaxation time τ is recorded for system A and system B at the peak of the conductivity curve which is expressed in Figure 4.10 (a) and Figure 4.10 (b), respectively.

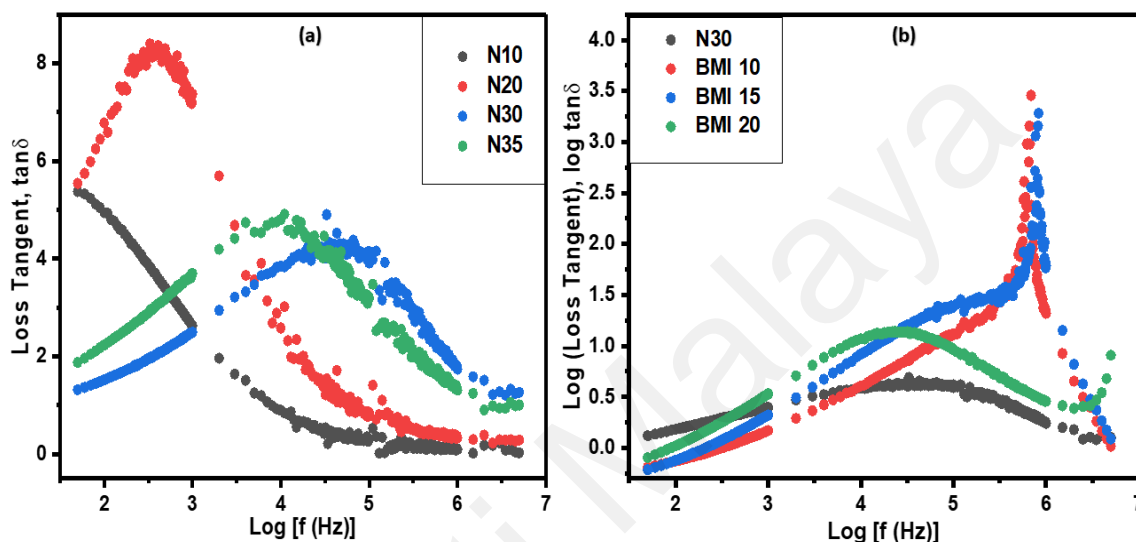


Figure 4.10: Variation of loss tangent versus $\log f$ plot for (a) System A and (b) System B respectively at room temperature.

As more concentration of the salt was incorporated, the amorphous region expanded and PAAC molecular structure became loose and weak. Polymeric chain became more flexible to orient, resulting a reduction in relaxation time. For PAAC: NaI, polymer electrolyte systems, the loss peak $\tan \delta$ shifted towards higher frequency region with increasing salt content until 30 wt.%, thus, reducing the relaxation time. It is often behaving as the resonance effect of an oscillator. In general, a resonance dipolar relaxation is expected to occur when the frequency of the applied electric field is comparable to the characteristic or natural frequency of the dipoles (Tiller, 1992). By taking Debye equation in an ideal case, and assuming the static dielectric constant and high frequency dielectric constant are almost the same (Chopra et al., 2003), the

segmental relaxation time τ can be calculated from the frequency, f_m corresponding to the peak according to equation 4.2;

$$\omega\tau = 2\pi f\tau = 1; \tau = \frac{1}{2\pi f} \quad (4.2)$$

Table 4.1 indicates that the lowest relaxation time of 3.73×10^{-6} s was observed for the sample A with salt concentration of N30 which led to the maximum DC ionic conductivity at room temperature. The low relaxation time indicates the faster ion migration from one coordinating site to another and hence high ionic conductivity. On the other hand, the results for the relaxation time for N10 sample was unable to be derived from the experiment because the peak of $\tan \delta$ was beyond frequency range of measuring instrument.

Table 4.1: The peak frequency, f_m and the relaxation time, τ for system A

| Sample A | Peak Frequency, f_m (Hz) | Relaxation time, τ (s) |
|----------|----------------------------|-----------------------------|
| N10 | – | – |
| N20 | 4.074×10^2 | 3.91×10^{-4} |
| N30 | 4.266×10^4 | 3.73×10^{-6} |
| N35 | 1.096×10^4 | 1.45×10^{-5} |

In comparison to analyses, the effect of adding ionic liquid BMI into the optimized system A, Table 4.2 indicates that the lowest relaxation time of 2.10×10^{-7} s was observed for the system B with the optimized ionic liquid BMI 15 wt. % which is consistent with highest DC ionic conductivity at room temperature.

Table 4.2: The peak frequency, f_m and the relaxation time, τ for system B

| Sample B | Peak Frequency, f_m (Hz) | Relaxation time, τ (s) |
|----------|----------------------------|-----------------------------|
| BMI 10 | 6.761×10^5 | 2.35×10^{-7} |
| BMI 15 | 7.586×10^5 | 2.10×10^{-7} |
| BMI 20 | 2.884×10^4 | 5.52×10^{-6} |

4.3.3 Temperature Dependent Tangent Loss Spectra Analysis

The plots of Loss Tangent of system A and system B with change in frequency are shown in Figures 4.11 at some selected temperatures 313 K, 323 K, 333 K, 343 K, 353K, 363and 373 K respectively.

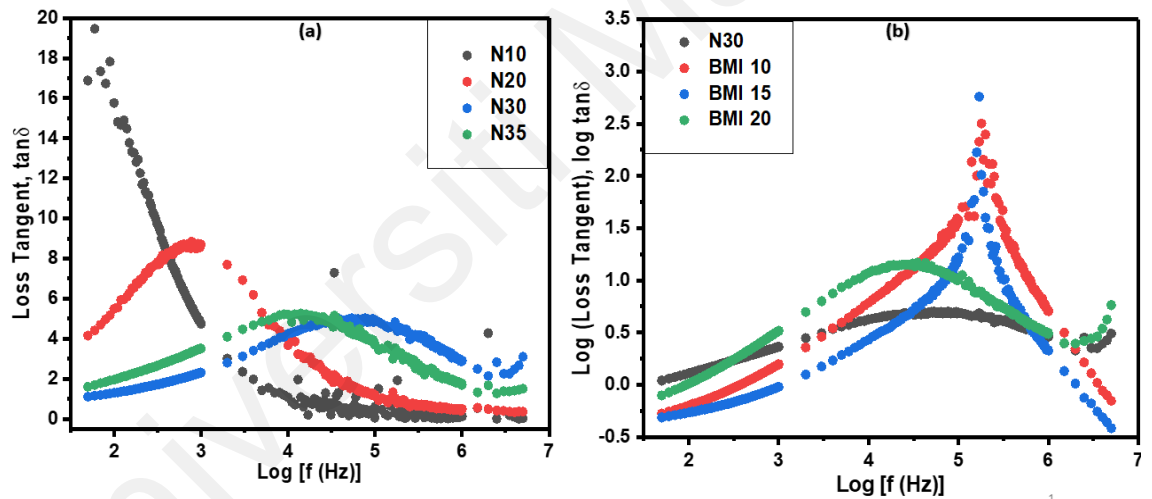


Figure 4.11: Variation of loss tangent versus log f plot for (a) System A and (b) System B respectively at 313 K.

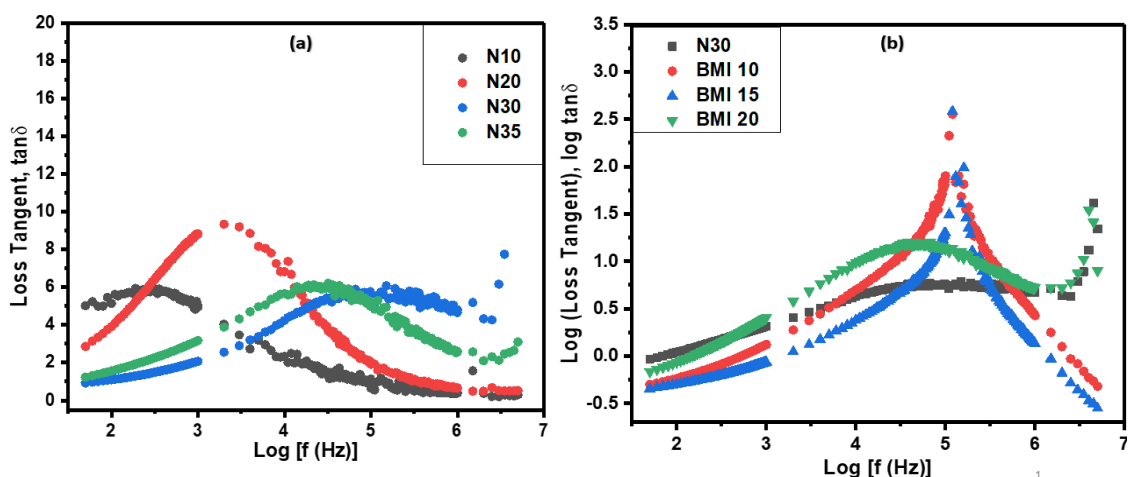


Figure 4.12: Variation of loss tangent versus log f plot for (a) System A and (b) System B respectively at 323 K.

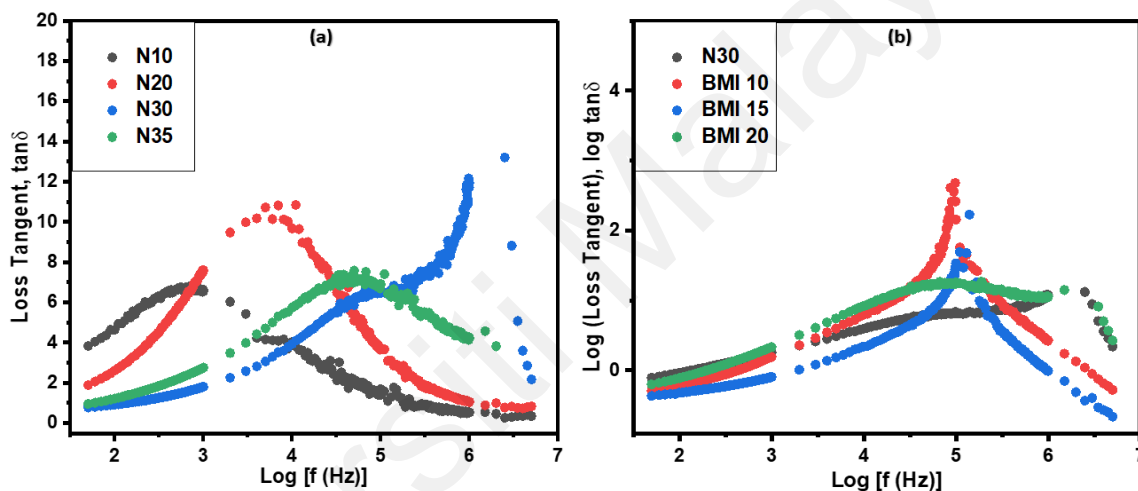


Figure 4.13: Variation of loss tangent versus log f plot for (a) System A and (b) System B respectively at 333K.

Figure 4.11 (a), Figure 4.12 (a), and Figure 4.13 (a) are comparing the Loss Tangent graphs for temperature ranges from 313 K until 333K, which clearly show the shortest segmental relaxation time observed for N30 sample of system A and similarly Figure 4.11 (b), Figure 4.12 (b) and Figure 4.13 (b) are indicating the shortest relaxation time observed for the optimized ionic liquid BMI 15 wt. % containing sample of system B.

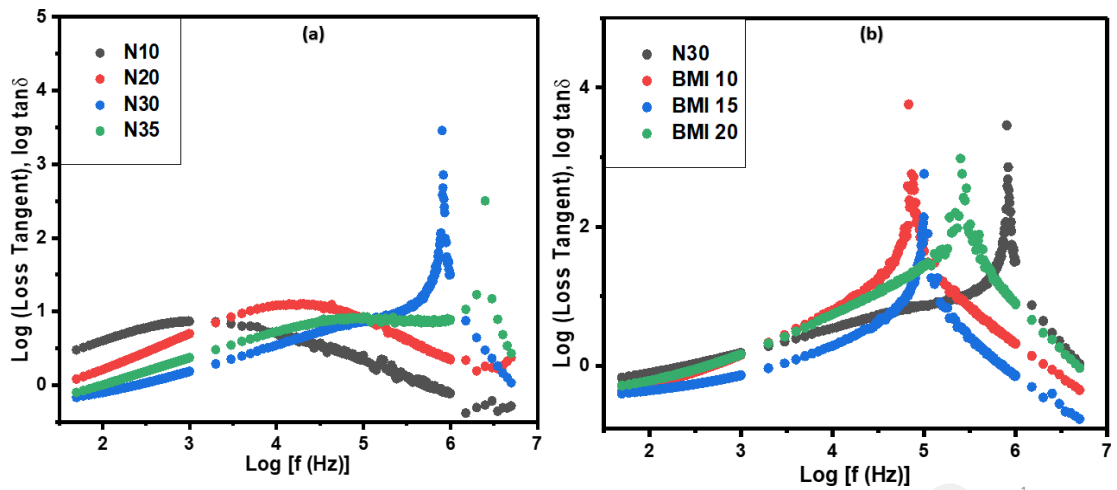


Figure 4.14: Variation of loss tangent versus log f plot for (a) System A and (b) System B respectively at 343K.

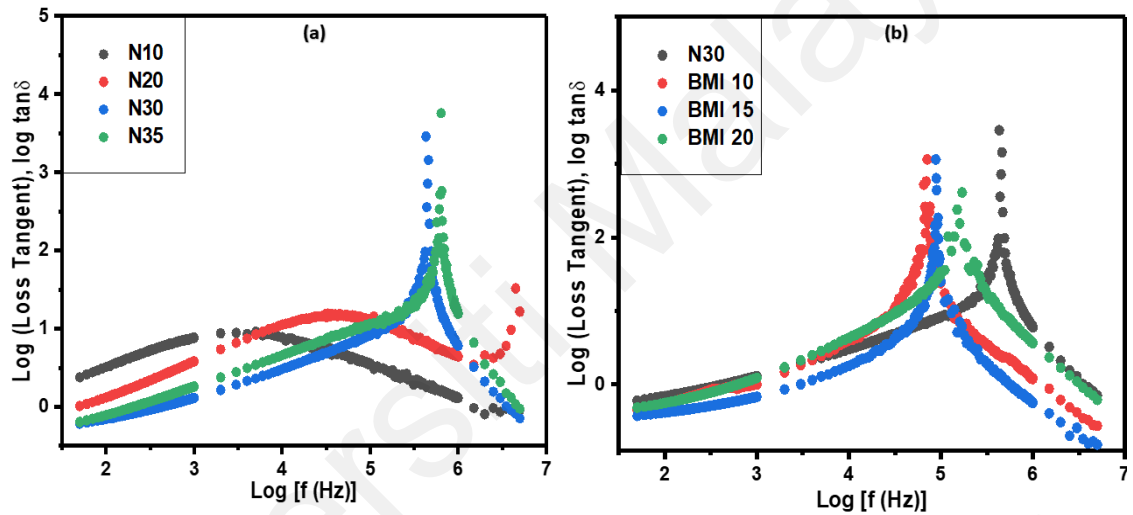


Figure 4.15: Variation of loss tangent versus log f plot for (a) System A and (b) System B respectively at 353K.

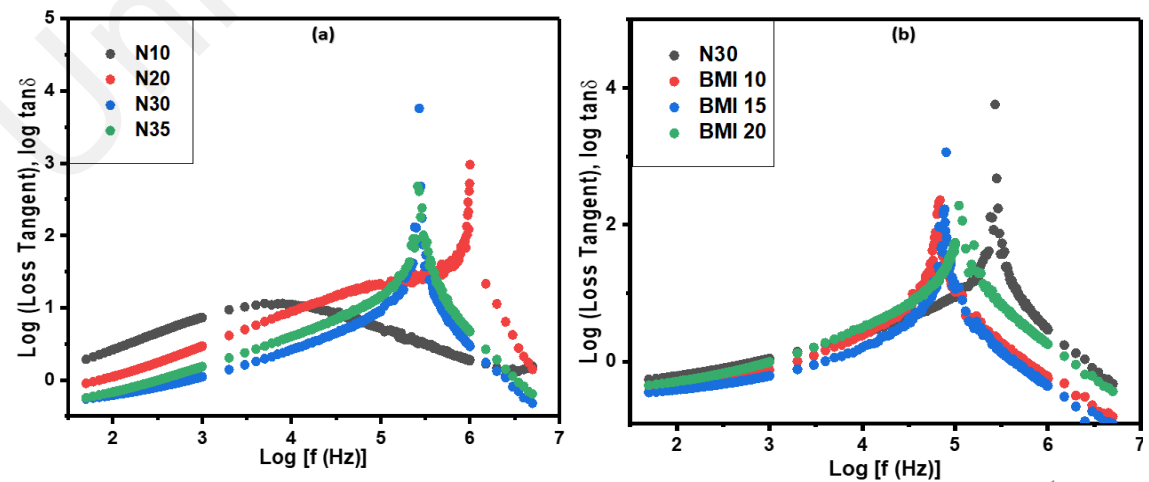


Figure 4.16: Variation of loss tangent versus log f plot for (a) System A and (b) System B respectively at 363K.

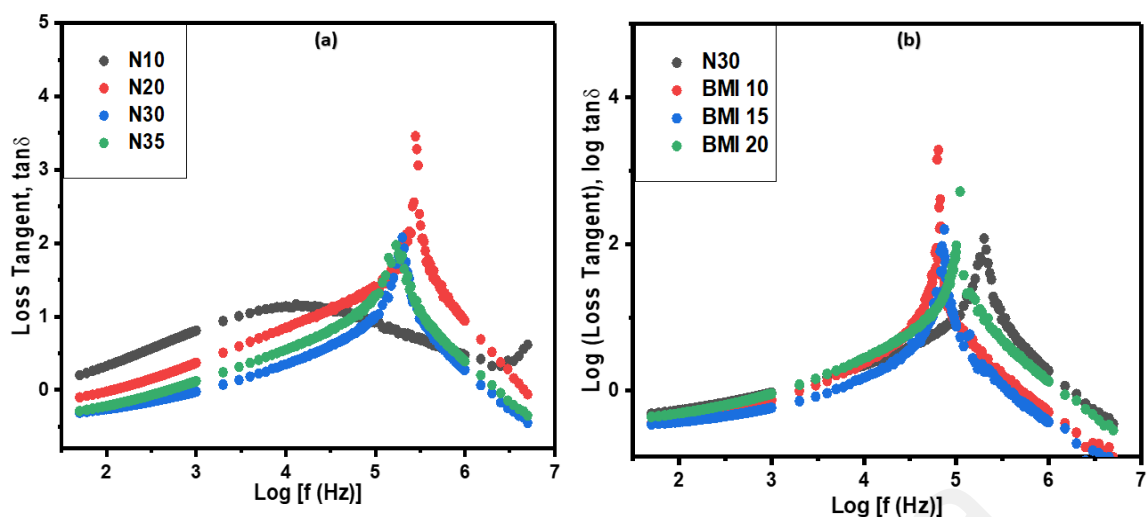


Figure 4.17: Variation of loss tangent versus log f plot for (a) System A and (a) System B respectively at 373K.

Figure 4.14 (a), Figure 4.15 (a), Figure 4.16 (a), and Figure 4.17 (a) comparing the Loss Tangent graphs for temperature ranges from 343K until 373K. It's clearly highlights how the segmental relaxation time varied as the temperature increases. It is also indicating that the segmental of motion of the PAAC has been significantly changed at high temperatures.

4.3.4 Modulus Electric Analysis at room temperature

Generally, both plots of M' and M'' show an increase at the higher frequency range. It has been observed that there are well-defined dispersion peaks in M'' plots which shows features of an ionic conduction (Hadi et al., 2020). Both M' and M'' decreased at low frequencies due to the negligible contribution of electrode polarization (Ramesh & Arof, 2001). In Figure 4.18 (a), the trend shows that M' approaches to zero at low frequency region and this long tail is attributed to the large capacitance associated with the electrode polarization. A similar result has been reported by Woo et al. (Woo et al., 2012). In the high frequency region, M' shows a sigmoidal shape for N10. As the salt content increased, the overall spectra were shifted to the right beyond the frequency window of this

experiment, thus showing the dispersion part, which demonstrate the reverse conductivity trend.

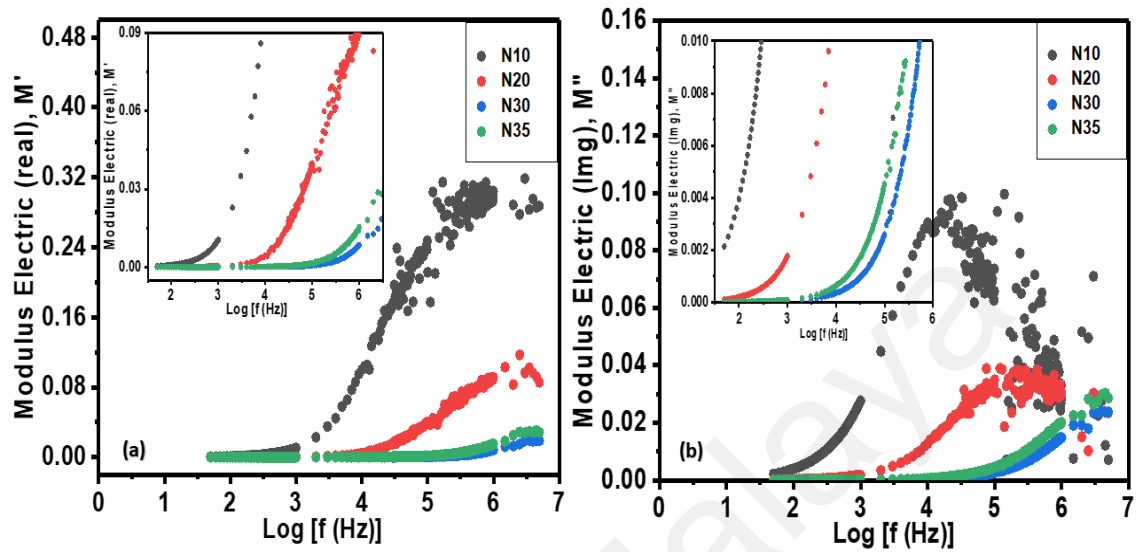


Figure 4.18: Variation of (a) M' versus $\log f$ and (b) Variation of M'' versus $\log f$ for different [PAAC-NaI] electrolyte system A at room temperature.

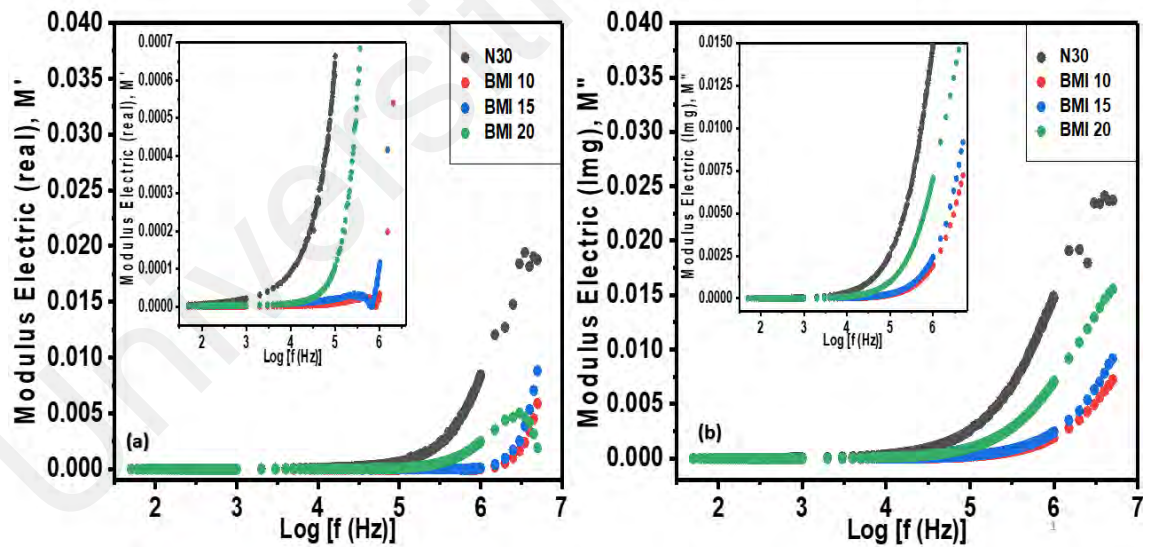


Figure 4.19: Variation of (a) M' versus $\log f$ and (b) Variation of M'' versus $\log f$ for different [PAAC-NaI-BMI] electrolyte system B at room temperature.

In Figure 4.18 (b), M'' plot presents a single, broad, and asymmetric peak in the high frequency region for N10 and N20 salt concentration. The single well-defined resonance peak is an indication of long-range conductivity relaxation in good ionic conductors. As more salt was added, the peak was shifted to the higher frequency region prior to the

shorter conduction relaxation time. Overall, the reduced value of conduction relaxation time accompanied with the tremendous increase in the M'' at the higher frequency region in Figure 4.18 (b) and Figure 4.19 (b) for system A and system B which can be related to the hopping of ions from one site to other site over a long distance with the natural jump frequency (Druger et al., 1985). When the frequency of the external field was matched with the natural frequency of the polymer electrolyte systems, maximum energy was transferred resulting due to the resonance effect. However, the asymmetric peak of the M'' in Figure 4.18 (b) clearly indicates the non-exponential behavior of the conductivity relaxation, which can be described by the Kohlrausch-Williams-Watts function (Williams & Watts, 1970).

4.3.5 Temperature Dependent Modulus Electric Analysis

It is also observed that with increasing the temperature, the value of real Modulus Electric M' and imaginary modulus Electric M'' decreases at high frequency region due to increase in mobility of charge carriers with temperature (Kumar et al., 2020). The value of M' and M'' in Figure 4.20 (a) and (b) shows the conduction relaxation peak shifts towards higher frequency with increasing temperature because of faster ionic motion, leading to decrease in the conductivity relaxation time. This also suggest that at higher frequency region of the M'' graphs in Figure 4.20 (b) & Figure 4.21 (b) for both system A and system B, the dispersion peaks shifted towards higher frequencies as the temperature increases (Aziz, Hamsan, et al., 2020). Where the dispersion effect as a result of bulk relaxation effect is expected to appear at frequency > 1 MHz. Once the dispersion effect was confirmed, the ionic conduction and polymer segmental relaxation were coupled together and resulted a single conduction relaxation peak in the M'' spectra.

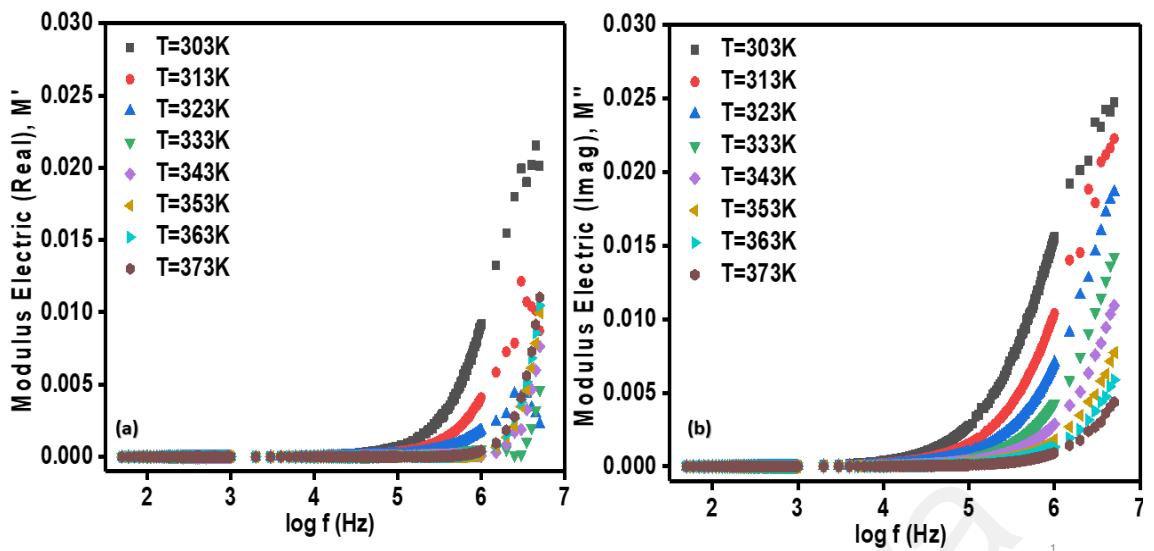


Figure 4.20: The temperature dependent (a) M' versus $\log f$ and (b) M'' versus $\log f$ respectively for optimized N30 electrolyte system A.

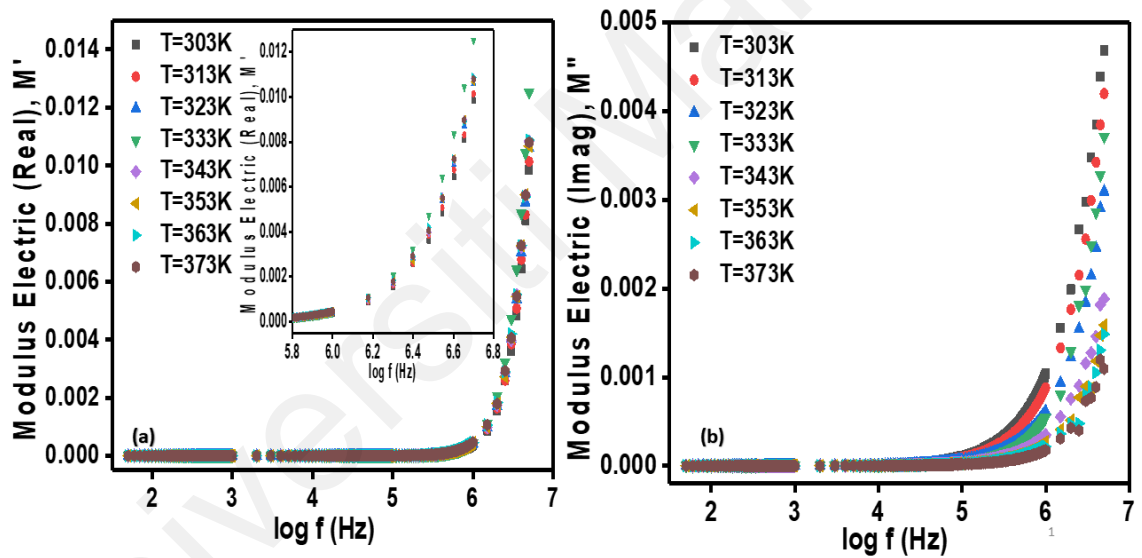


Figure 4.21: The temperature dependent (a) M' versus $\log f$ and (b) M'' versus $\log f$ respectively for optimized BMI15 electrolyte system B.

CHAPTER 5: CONCLUSIONS AND FUTURE WORK

5.1 Conclusions

The polymer electrolyte thin films based on Poly (acrylamide-co-acrylic acid) (PAAC) has been prepared successfully with solution casting method by adding sodium iodide salt with various weight percentage (System A) and other thin films has been prepared by optimizing system with adding ionic liquid of 1-Butyl-3-Methylimidazolium Iodide (BMI) (System B). In both systems, the highest ionic conductivity evaluated $1.88 \times 10^{-5} \text{ Scm}^{-1}$ at room temperature for the 30% NaI salt-doped polymer electrolyte for system A with the lowest activation energy of 0.48 eV were attained and the conductivity optimized up to maximum value of $4.73 \times 10^{-4} \text{ Scm}^{-1}$ at room temperature for the system B containing 15% ionic liquid BMI with lowest activation energy of 0.26 eV were observed.

For both system A and system B, the temperature dependent DC conductivity obeys Arrhenius relationship which indicates the DC conductivity increases gradually as the temperature increases due to the cation transport mechanism. As the temperature increased, the vibrational energy of a polymer chain caused the amorphous phase expansion and induced the segmental motion, which exhibited the shortest relaxation time for the optimized samples N30 and BMI up to 333K.

In conclusion, the transport properties of host polymer Poly (acrylamide-co-acrylic acid) (PAAC) added with salt and ionic liquids has shown increasing trend of DC conductivity and exhibited high dielectric constant with long range conductivity relaxation of modulus electric as the temperature increased.

5.2 Future Work

The transport properties and segmental dynamics of the host polymer especially at high temperatures of Poly (acrylamide-co-acrylic acid) (PAAC) can be further investigated. The results of Loss Tangent analysis indicated for the optimized samples

with salt (System A) and ionic liquid (System B) show the segmental relaxation time showing increasing trend above 333K temperature. Future work can be established to study and understand the molecular dynamics of segmental motion correlated with cationic motion to optimize the transport properties at the high temperature region.

Universiti Malaya

REFERENCES

- Agrawal, R. C., & Pandey, G. P. (2008). Solid polymer electrolytes: Materials designing and all-solid-state battery applications: An overview. *Journal of Physics D: Applied Physics*, *41*(22).
- Ahmad, A., Isa, K. B. M., & Osman, Z. (2011). Conductivity and structural studies of plasticized polyacrylonitrile (PAN) -Lithium triflate polymer electrolyte films. *Sains Malaysiana*, *40*(7), 691–694.
- Avellaneda, C. O., Vieira, D. F., Al-Kahlout, A., Leite, E. R., Pawlicka, A., & Aegerter, M. A. (2007). Solid-state electrochromic devices with Nb₂O₅:Mo thin film and gelatin-based electrolyte. *Electrochimica Acta*, *53*(4), 1648–1654.
- Awadhia, A., & Agrawal, S. L. (2007). Structural, thermal and electrical characterizations of PVA:DMSO:NH₄SCN gel electrolytes. *Solid State Ionics*, *178*(13–14), 951–958.
- Aziz, S. B., Brevik, I., Hamsan, M. H., Brza, M. A., M. Nofal, M., Abdullah, A. M., Rostam, S., Al-Zangana, S., Muzakir, S. K., & Kadir, M. F. Z. (2020). Compatible Solid Polymer Electrolyte Based on Methyl Cellulose for Energy Storage Application: Structural, Electrical, and Electrochemical Properties. *Polymers*, *12*(10), Article#2257.
- Aziz, S. B., Hamsan, M. H., Kadir, M. F. Z., & Woo, H. J. (2020). Design of polymer blends based on chitosan:POZ with improved dielectric constant for application in polymer electrolytes and flexible electronics. *Advances in Polymer Technology*, *2020*.
- Aziz, S. B., Woo, T. J., Kadir, M. F. Z., & Ahmed, H. M. (2018). A conceptual review on polymer electrolytes and ion transport models. In *Journal of Science: Advanced Materials and Devices* (Vol. 3, Issue 1, pp. 1–17). Elsevier B.V.
- Campbell, J. A., Goodwin, A. A., & Simon, G. P. (2001). Dielectric relaxation studies of miscible polycarbonate/polyester blends. *Polymer*, *42*(10), 4731–4741.
- Carvalho, L. M., Guégan, P., Cheradame, H., & Gomes, A. S. (2000). Variation of the mesh size of PEO-based networks filled with TFSILi: from an Arrhenius to WLF type conductivity behavior. *European Polymer Journal*, *36*(2), 401–409.
- Chong, M. Y., Liew, C. W., Numan, A., Yugal, K., Ramesh, K., Ng, H. M., Chong, T. V., & Ramesh, S. (2016). Effects of ionic liquid on the hydroxylpropylmethyl cellulose (HPMC) solid polymer electrolyte. *Ionics*, *22*(12), 2421–2430.
- Chong, M. Y., Numan, A., Liew, C. W., Ramesh, K., & Ramesh, S. (2017). Comparison of the performance of copper oxide and yttrium oxide nanoparticle based hydroxylethyl cellulose electrolytes for supercapacitors. *Journal of Applied Polymer Science*, *134*(13), 1–11.
- Chopra, S., Sharma, S., Goel, T. C., & Mendiratta, R. G. (2003). Structural, dielectric and pyroelectric studies of Pb_{1-x}Ca_xTiO₃ thin films. *Solid State Communications*, *127*(4), 299–304.

- Cole, K. S., & Cole, R. H. (1941). Dispersion and absorption in dielectrics I. Alternating current characteristics. *The Journal of Chemical Physics*, 9(4), 341–351.
- Dhatarwal, P., & Sengwa, R. J. (2020). Dielectric relaxation, Li-ion transport, electrochemical, and structural behaviour of PEO/PVDF/LiClO₄/TiO₂/PC-based plasticized nanocomposite solid polymer electrolyte films. *Composites Communications*, 17(December 2019), 182–191.
- Diddens, D., Heuer, A., & Borodin, O. (2010). Understanding the lithium transport within a rouse-based model for a PEO/LiTFSI polymer electrolyte. *Macromolecules*, 43(4), 2028–2036.
- Druger, S. D., Ratner, M. A., & Nitzan, A. (1985). Generalized hopping model for frequency-dependent transport in a dynamically disordered medium, with applications to polymer solid electrolytes. *Physical Review B*, 31(6), 3939–3947. <https://doi.org/10.1103/PhysRevB.31.3939>
- Fattah, N. F. A., Ng, H. M., Mahipal, Y. K., Numan, A., Ramesh, S., & Ramesh, K. (2016). An approach to solid-state electrical double layer capacitors fabricated with graphene oxide-doped, ionic liquid-based solid copolymer electrolytes. *Materials*, 9(6).
- Gueye, M. N., Carella, A., Faure-Vincent, J., Demadrille, R., & Simonato, J. P. (2020). Progress in understanding structure and transport properties of PEDOT-based materials: A critical review. *Progress in Materials Science*, 108, Article#100616.
- Hadi, J. M., Aziz, S. B., Nofal, M. M., Hussien, S. A., Hamsan, M. H., Brza, M. A., Abdulwahid, R. T., Kadir, M. F. Z., & Woo, H. J. (2020). Electrical, dielectric property and electrochemical performances of plasticized silver ion-conducting chitosan-based polymer nanocomposites. *Membranes*, 10(7), 1–22.
- Hassan, M. F., & Arof, A. K. (2005). Ionic conductivity in PEO-KOH polymer electrolytes and electrochemical cell performance. *Physica Status Solidi (A) Applications and Materials Science*, 202(13), 2494–2500.
- Hassan, Mohd Faiz, & Yusof, S. Z. M. (2014). Poly(Acrylamide-Co-Acrylic Acid)-Zinc Acetate polymer electrolytes: Studies based on structural and morphology and electrical spectroscopy. *Microscopy Research*, 02(02), 30–38.
- Hayamizu, K., Sugimoto, K., Akiba, E., Aihara, Y., Bando, T., & Price, W. S. (2002). An NMR and ionic conductivity study of ion dynamics in liquid poly(ethylene oxide)-based electrolytes doped with LiN(SO₂CF₃)₂. *Journal of Physical Chemistry B*, 106(3), 547–554.
- Hougham, G., Tesoro, G., Viehbeck, A., & Chapple-Sokol, J. D. (1994). Polarization effects of fluorine on the relative permittivity in polyimides. *Macromolecules*, 27(21), 5964–5971.
- J.Y.Cherng, M.Z.A.Munshi, B. B. O. A. W. H. S. (1987). Applications of multivalent ionic conductors to polymeric electrolyte batteries. *Solid State Ionics*, 28–30, 857–861.

- Kaiser, A. B. (2001). Electronic transport properties of conducting polymers and carbon nanotubes. *Reports on Progress in Physics*, 64(1), 1–49.
- Kim, J. S. (2001). Electric modulus spectroscopy of lithium tetraborate (Li₂B₄O₇) single crystal. *Journal of the Physical Society of Japan*, 70(10), 3129–3133.
- Klein, R. J., Zhang, S., Dou, S., Jones, B. H., Colby, R. H., & Runt, J. (2006). Modeling electrode polarization in dielectric spectroscopy: Ion mobility and mobile ion concentration of single-ion polymer electrolytes. *Journal of Chemical Physics*, 124(14).
- Koops, C. G. (1951). On the dispersion of resistivity and dielectric constant of some semiconductors at audiofrequencies. *Physical Review*, 83(1), 121–124.
- Kumar, A., Madaan, M., Arya, A., Tanwar, S., & Sharma, A. L. (2020). Ion transport, dielectric, and electrochemical properties of sodium ion-conducting polymer nanocomposite: application in EDLC. *Journal of Materials Science: Materials in Electronics*, Article#0123456789.
- Kumar, D., Gohel, K., Kanchan, D. K., & Mishra, K. (2020). Dielectrics and battery studies on flexible nanocomposite gel polymer electrolyte membranes for sodium batteries. *Journal of Materials Science: Materials in Electronics*, Article#0123456789.
- Lan, Z., Wu, J., Lin, J., Huang, M., Yin, S., & Sato, T. (2007). Influence of molecular weight of PEG on the property of polymer gel electrolyte and performance of quasi-solid-state dye-sensitized solar cells. *Electrochimica Acta*, 52(24), 6673–6678.
- Li, L., Liu, L., Qing, Y., Zhang, Z., Yan, N., Wu, Y., & Tian, C. (2018). Stretchable alkaline poly(acrylic acid) electrolyte with high ionic conductivity enhanced by cellulose nanofibrils. *Electrochimica Acta*, 270, 302–309.
- Ling, C. K., Aung, M. M., Abdullah, L. C., Hong Ngee, L., & Uyama, H. (2020). A short review of iodide salt usage and properties in dye sensitized solar cell application: Single vs binary salt system. *Solar Energy*, 206(April), 1033–1038.
- Louati, B., Hlel, F., & Guidara, K. (2009). Ac electrical properties and dielectric relaxation of the new mixed crystal (Na_{0.8}Ag_{0.2})₂PbP₂O₇. *Journal of Alloys and Compounds*, 486(1–2), 299–303.
- Macdonald JR. (1992). Impedance spectroscopy. *Annals of Biomedical Engineering*, 20(9), 289–305.
- Michael, M. S., Jacob, M. M. E., Prabakaran, S. R. S., & Radhakrishna, S. (1997). Enhanced lithium ion transport in PEO-based solid polymer electrolytes employing a novel class of plasticizers. *Solid State Ionics*, 98(3–4), 167–174.
- Mishra, R., & Rao, K. J. (1998). Electrical conductivity studies of poly(ethyleneoxide)-poly(vinylalcohol) blends. *Solid State Ionics*, 106(1–2), 113–127.

- Munar, A., Andrio, A., Iserte, R., & Compañ, V. (2011). Ionic conductivity and diffusion coefficients of lithium salt polymer electrolytes measured with dielectric spectroscopy. *Journal of Non-Crystalline Solids*, 357(16–17), 3064–3069.
- Nithya, S., Selvasekarapandian, S., Karthikeyan, S., Inbavalli, D., Sikkinthar, S., & Sanjeeviraja, C. (2014). AC impedance studies on proton-conducting PAN: NH₄SCN polymer electrolytes. *Ionics*, 20(10), 1391–1398.
- Pradhan, D. K., Choudhary, R. N. P., & Samantaray, B. K. (2008). Studies of dielectric relaxation and AC conductivity behavior of plasticized polymer nanocomposite electrolytes. *International Journal of Electrochemical Science*, 3(5), 597–608.
- Przyłuski, J., & Wieczorek, W. (1989). Increasing the conductivity of polymer solid electrolytes: A review. *Solid State Ionics*, 36(3–4), 165–169.
- Ramesh, S., & Arof, A. K. (2001). Ionic conductivity studies of plasticized poly(vinyl chloride) polymer electrolytes. *Materials Science and Engineering B: Solid-State Materials for Advanced Technology*, 85(1), 11–15.
- Ravi, M., Pavani, Y., Kiran Kumar, K., Bhavani, S., Sharma, A. K., & Narasimha Rao, V. V. R. (2011). Studies on electrical and dielectric properties of PVP:KBrO₄ complexed polymer electrolyte films. *Materials Chemistry and Physics*, 130(1–2), 442–448.
- Sangeetha, M., Mallikarjun, A., Aparna, Y., Reddy, M. V., Kumar, J. S., Sreekanth, T., & Reddy, M. J. (2021). Dielectric studies and AC conductivity of PVDF-HFP: LiBF₄: EC plasticized polymer electrolytes. *Materials Today: Proceedings*, 44(xxxx), 2168–2172.
- Sangeetha, M., Mallikarjun, A., Jaipal Reddy, M., & Siva Kumar, J. (2017). FTIR Spectroscopic and DC Ionic conductivity Studies of PVDF-HFP: LiBF₄: EC Plasticized Polymer Electrolyte Membrane. *IOP Conference Series: Materials Science and Engineering*, 225(1).
- Schütt, H. J., & Gerdes, E. (1992). Space-charge relaxation in ionically conducting oxide glasses. I. Model and frequency response. *Journal of Non-Crystalline Solids*, 144(C), 1–13.
- Selvasekarapandian, S., Baskaran, R., & Hema, M. (2005). Complex AC impedance, transference number and vibrational spectroscopy studies of proton conducting PVAc-NH₄SCN polymer electrolytes. *Physica B: Condensed Matter*, 357(3–4), 412–419.
- Singh, P., Gupta, P. N., & Saroj, A. L. (2020). Ion dynamics and dielectric relaxation behavior of PVA-PVP-NaI-SiO₂ based nano-composites polymer blend electrolytes. *Physica B: Condensed Matter*, 578(July 2019), Article#411850.
- Singh, P. K., Bhattacharya, B., Nagarale, R. K., Pandey, S. P., Kim, K. W., & Rhee, H. W. (2010). Ionic liquid doped poly(N-methyl 4-vinylpyridine iodide) solid polymer electrolyte for dye-sensitized solar cell. *Synthetic Metals*, 160(9–10), 950–954.

- Singh, P. K., Kim, K. W., & Rhee, H. (2009). Electrochemistry Communications Quantum dot doped solid polymer electrolyte for device application. *Electrochemistry Communications*, 11(6), 1247–1250.
- Siva Kumar, J., Subrahmanyam, A. R., Jaipal Reddy, M., & Subba Rao, U. V. (2006). Preparation and study of properties of polymer electrolyte system (PEO + NaClO₃). *Materials Letters*, 60(28), 3346–3349. <https://doi.org/10.1016/j.matlet.2006.03.015>
- Stamenković, J. V., Premović, P. I., & Mentus, S. V. (1997). Electrical conductivity of poly(acrylic acid) gels. *Journal of the Serbian Chemical Society*, 62(10), 945–950.
- Świergiel, J., & Jadżyn, J. (2011). Electric relaxational effects induced by ionic conductivity in dielectric materials. *Industrial and Engineering Chemistry Research*, 50(21), 11935–11941.
- Tan, C. Y., Saidi, N. M., Farhana, N. K., Omar, F. S., Algaradah, M. M., Bashir, S., Ramesh, S., & Ramesh, K. (2020). Improved ionic conductivity and efficiency of dye-sensitized solar cells with the incorporation of 1-methyl-3-propylimidazolium iodide. *Ionics*, 26(6), 3173–3183.
- Tang, Z., Wu, J., Liu, Q., Zheng, M., Tang, Q., Lan, Z., & Lin, J. (2012). Preparation of poly(acrylic acid)/gelatin/polyaniline gel-electrolyte and its application in quasi-solid-state dye-sensitized solar cells. *Journal of Power Sources*, 203, 282–287.
- Tiller, A. R. (1992). Dielectric relaxation in polymers by molecular dynamics simulation. *Macromolecules*, 25(18), 4605–4611.
- Wan, Y., Creber, K. A. M., Peppley, B., & Bui, V. T. (2003). Ionic conductivity of chitosan membranes. *Polymer*, 44(4), 1057–1065.
- Wang, Jingping, Xu, Y., Wang, J., Zhu, J., Bai, Y., & Xiong, L. (2014). Study on capacitance evolving mechanism of polypyrrole during prolonged cycling. *Journal of Physical Chemistry B*, 118(5), 1353–1362.
- Wang, Jingwei, Chen, G., & Song, S. (2020). Na-ion conducting gel polymer membrane for flexible supercapacitor application. *Electrochimica Acta*, 330, Article#135322.
- Wang, Y. (2009). Recent research progress on polymer electrolytes for dye-sensitized solar cells. In *Solar Energy Materials and Solar Cells* (Vol. 93, Issue 8, pp. 1167–1175).
- Wieczorek, W., & Stevens, J. R. (1997). Impedance spectroscopy and phase structure of polyether-poly(methyl methacrylate)-LiCF₃SO₃ blend-based electrolytes. *Journal of Physical Chemistry B*, 101(9), 1529–1534.
- Wieczorek, W., Such, K., Florjanczyk, Z., & Stevens, J. R. (1995). Polyacrylamide based composite polymeric electrolytes. *Electrochimica Acta*, 40(13–14), 2417–2420.
- Williams, G., & Watts, D. C. (1970). Non-symmetrical dielectric relaxation behaviour arising from a simple empirical decay function. *Transactions of the Faraday Society*, 66(1), 80–85.

- Woo, H. J., Majid, S. R., & Arof, A. K. (2012). Dielectric properties and morphology of polymer electrolyte based on poly(ϵ -caprolactone) and ammonium thiocyanate. *Materials Chemistry and Physics*, 134(2–3), 755–761.
- Wright, P. V. (1975). Electrical conductivity in ionic complexes of poly(ethylene oxide). *British Polymer Journal*, 7(5), 319–327.
- Zhang, H. P., Zhang, P., Li, Z. H., Sun, M., Wu, Y. P., & Wu, H. Q. (2007). A novel sandwiched membrane as polymer electrolyte for lithium ion battery. *Electrochemistry Communications*, 9(7), 1700–1703.
- Zhu, W., Wang, X., Yang, B., & Tang, X. (2001). *A Novel Ionic-Conduction Mechanism Based on. March*, 1246–1254.

Universiti Malaya